Title: Multi-species genome-wide CRISPR screens identify conserved suppressors of cold-induced cell death

Authors

Breanna Lam[1,*], Kathrin M. Kajderowicz[1,2,*], Heather R. Keys[1], Julian M. Roessler[1], Evgeni M. Frenkel[1], Adina Kirkland[1], Punam Bisht[1], Mohamed A. El-Brolosy[1,3], Rudolf Jaenisch[1], George W. Bell[1], Jonathan S. Weissman[1], Eric C. Griffith[4], Sinisa Hrvatin[1,†]

Affiliations

[1]Whitehead Institute for Biomedical Research and Department of Biology, Massachusetts Institute of Technology, Cambridge, MA 02142, USA

[2]Department of Brain and Cognitive Sciences, Massachusetts Institute of Technology, Cambridge, MA 02142, USA

[3]Harvard Society of Fellows, Cambridge, MA, 02138, USA

[4]Department of Neurobiology, Harvard Medical School, Boston, MA 02115, USA

*These two authors contributed equally to this work

Corresponding author

[†]Sinisa Hrvatin (shrvatin@wi.mit.edu)

Summary

Cells must adapt to environmental changes to maintain homeostasis. One of the most striking environmental adaptations is entry into hibernation during which core body temperature can decrease from 37°C to as low at 4°C. How mammalian cells, which evolved to optimally function within a narrow range of temperatures, adapt to this profound decrease in temperature remains poorly understood. In this study, we conducted the first genome-scale CRISPR-Cas9 screen in cells derived from Syrian hamster, a facultative hibernator, as well as human cells to investigate the genetic basis of cold tolerance in a hibernator and a non-hibernator in an unbiased manner. Both screens independently revealed glutathione peroxidase 4 (GPX4), a selenium-containing enzyme, and associated proteins as critical for cold tolerance. We utilized genetic and pharmacological approaches to demonstrate that GPX4 is active in the cold and its catalytic activity is required for cold tolerance. Furthermore, we show that the role of GPX4 as a suppressor of cold-induced cell death extends across hibernating species, including 13-lined ground squirrels and greater horseshoe bats, highlighting the evolutionary conservation of this

mechanism of cold tolerance. This study identifies GPX4 as a central modulator of mammalian cold tolerance and advances our understanding of the evolved mechanisms by which cells mitigate cold-associated damage—one of the most common challenges faced by cells and organisms in nature.

Introduction

Rapid temperature changes pose a challenge to all clades of life, including endotherms. Homeotherms such as mammals routinely defend a core body temperature set-point, with profound thermal deviations leading to organ dysfunction and death[1–4]. Indeed, several studies have shown that while homeotherm-derived cells typically possess a capacity for mild cold tolerance in culture, primary cultured cells and cell lines derived from a number of mammalian species, including humans, exhibit high rates of cell death following prolonged severe cold exposure[5–8]. Although considerable work has focused on understanding the cellular responses and adaptations to an increased temperature (heat stress and heat-shock)[9–11], little is known about how cell biological processes modulate cell sensitivity to decreased temperatures.

The mechanisms underlying cold-induced death remain poorly understood but have been hypothesized to involve phase transition of cellular membranes, with the resulting membrane damage leading to ion gradient disruption and irrecoverable cellular dysfunction[12–15]. However, many warm-blooded animals, including some primates, have evolved the ability to enter torpor and hibernation – states during which body temperature can decrease far below its homeostatic set-point[16–18]. In many animals, *torpor* is a state of profoundly reduced metabolic rate and body temperature lasting from hours to days, while *hibernation* is a seasonal behavior comprising multiple bouts of *torpor* interrupted by periodic arousals to normal body temperature. During torpor, the core body temperature of many small hibernators including the Syrian golden hamster (*Mesocricetus auratus*), the 13-lined ground squirrel (*Ictidomys tridecemlineatus*), and the greater horseshoe bat (*Rhinolophus ferrumequinum*), reaches 4-10°C[19–21]. Animals can remain at these low temperatures for extended periods of time (up to several weeks), indicating that their cells and tissues are either genetically predisposed to cold tolerance, or that they can adapt to tolerate long-term cold exposure[19–22].

Although in principle the ability to tolerate cold temperatures could be conveyed by systemic factors present in torpid or hibernating animals, cell lines derived from hibernating rodents maintain high viability when exposed to 4°C for several days, indicating the presence of cell-

69 intrinsic mechanisms of cold tolerance[5–8]. Several studies have reported distinctive responses of
70 hibernator-derived cells in the cold. For example, Syrian hamster-derived epithelial-like hamster
71 kidney (HaK) cells maintain mitochondrial membrane potential and ATP production during cold
72 exposure[7], and both HaK and epithelial-like smooth muscle cells derived from the Syrian golden
73 hamster are able to prevent excess reactive oxygen species damage in response to cold
74 exposure[5]. Similarly, unlike human induced pluripotent stem cell (iPSC)-derived neurons, cultures
75 of iPSC-derived neurons from 13-lined ground squirrels retain microtubule stability in the cold[6].
76 Despite metabolic and cell biological differences between various hibernator and non-hibernator-
77 derived cells in the context of cold exposure, the underlying genetic modulators of cold tolerance
78 have yet to be systematically explored. Additionally, it is still unknown to what extent the pathways
79 that regulate cold tolerance in one hibernating species are conserved across other evolutionarily
80 distant hibernators and potentially even present in non-hibernators.
81
82 Here, we carry out the first unbiased genome-scale CRISPR-Cas9 screens in cells derived from
83 a cold-tolerant hibernator (Syrian hamster) as well as human (non-hibernator) cells to identify
84 genetic pathways required for long-term cold tolerance. Surprisingly, these screens independently
85 identify a common mechanism dependent on the selenocysteine-containing enzyme Glutathione
86 Peroxidase 4 (GPX4) as a key mediator of cellular cold tolerance. Employing genetic and
87 pharmacological approaches, we confirm these findings and demonstrate that increased GPX4
88 activity is sufficient to improve cold tolerance in human cells. We further show that functional
89 GPX4 is required for cold tolerance across several hibernating and non-hibernating mammals,
90 including in distantly related hibernating horseshoe bats (*Rhinolophus ferrumequinum*), and
91 propose that the GPX4 pathway may be a widespread, evolutionarily ancient metazoan
92 mechanism of cold tolerance across endotherms.
93
94 **Results**
95
96 **Assay for measuring viability of cold-exposed cells**
97 Our initial evaluation of the ability of human K562 leukemia cells to tolerate prolonged exposure
98 to extreme cold (4°C) temperatures led us to establish a new method for assessing viability of
99 cold-exposed cells. To avoid confounding changes in media composition or pH, we transferred
100 cultured cells into incubators cooled to 4°C with the CO_2 concentration calibrated to maintain
101 physiological pH (7.4). Cell survival was assessed based on exclusion of trypan blue, a
102 membrane-impermeable dye, immediately upon removal from 4°C. We observed a 27 ± 3%

survival rate for K562 cells following 24 hours at 4°C using this approach. However, recounting live cells after a 24-hour rewarming at 37°C revealed a ~6-fold increase in live cells, inconsistent with the reported 16-24 hour doubling rate of this cell line (**Figure 1b, Figure S1a**). Reasoning that a substantial fraction of trypan blue-positive cells at 4°C remain alive and capable of cell division and recovery upon rewarming, we carried out a time course of trypan blue staining shortly after removal from 4°C (**Figure 1a**). We found that the fraction of trypan blue-positive cells dramatically reduced following a brief rewarming period (30 minutes to 1 hour, either at room temperature or at 37°C), consistent with the number of live cells observed after 24 hours of rewarming (**Figure 1b,c, Figure S1a,b**). To determine whether this effect was isolated to K562 cells, we measured trypan blue-positive cells at 4°C or following a brief period of rewarming in several human cell lines (HEK 293T, HeLa, and RPE1 cells), as well as Syrian hamster kidney fibroblasts (BHK-21 cells) (**Figure S1c-f**). We consistently observed that, absent a rewarming period, trypan blue staining significantly overestimates cold-induced cell death. We thus adopted this brief rewarming period (~30-minutes) as a standard assay to measure cell viability of cold-exposed cells in our subsequent studies.

Hibernator-derived cells show enhanced cold tolerance compared to human cells

Using our modified assay for cell viability after cold challenge, we examined the relative cold tolerance of hibernator and non-hibernator cells. We tested four commonly used human cell lines (HT1080, HeLa, RPE1, and K562), as well as two cell lines (BHK-21 and HaK) derived from Syrian hamsters (*Mesocricetus auratus*), a hibernating mammal. Cells were placed at 4°C - the lower end of the temperature range which Syrian hamsters reach during hibernation - and we assessed cell survival after 1, 4, and 7 days of cold exposure. Consistent with prior reports[5,7,8], hamster-derived cell lines maintained high levels of viability, whereas human cell lines showed varying degrees of death (**Figures 1d-f**), with several exhibiting less than 50% survival following 7 days in the cold. Notably, we observed generally higher cell survival rates than previously reported[5], likely owing to our modified method of measuring cell viability. Similar survival trends were also observed using an orthogonal assay based on lactate dehydrogenase (LDH) release from dead cells into the media (**Figure 1g**).

Genome-scale CRISPR screen in a hibernator-derived cell line identifies suppressors of cold-induced cell death

To investigate the molecular pathways regulating cold resistance in hibernator-derived BHK-21 cells, we designed a genome-scale CRISPR-Cas9 screen. Taking advantage of a recent

137 chromosome-level assembly of the *Mesocricetus auratus* genome[23] and a modified CRISPOR-
138 based guide selection algorithm (Methods), we generated a library of 218,143 single guide RNAs
139 (sgRNAs) targeting all 21,473 annotated genes (~10 guides per gene), including 2,299 intergenic-
140 targeting and 250 non-targeting sgRNAs as negative controls. The pooled library was introduced
141 into BHK-21 cells via a lentiviral vector expressing the sgRNA along with Cas9, achieving ~1000-
142 fold library representation with a multiplicity of infection (MOI) < 1.
143
144 Considering that many mammalian species, including Syrian hamsters, undergo prolonged
145 periods of cold exposure (deep torpor) and rewarming (interbout arousals) during seasonal
146 hibernation, we sought to recapitulate these temperature changes in our screen. We thus exposed
147 BHK-21 cells to three cycles consisting of 4°C cold exposure (4 days) followed by rewarming at
148 37°C (2 days) ("4°C Cycling", **Figure 2a**). To isolate genes selectively required upon cold
149 exposure, we also analyzed BHK-21 cultures transduced in parallel that were maintained at 37°C
150 for four passages/cycles ("37°C Control", **Figure 2a**). For both paradigms, genomic DNA was
151 isolated from cells during each cycle/passage to monitor selective sgRNA depletion. To assess
152 our screen performance, we tested whether sgRNAs targeting previously identified human core
153 essential genes[24] were significantly depleted compared with nontargeting and intergenic sgRNAs
154 and found that we can robustly distinguish between these functional categories at all three cycles
155 and at both 37°C and 4°C (estimated p-value < 2.2e-16) (**Figure S2**).
156
157 To identify genes that selectively modify (suppress or potentiate) cold-induced cell loss, we
158 compared the guides depleted during three cycles of cold exposure and rewarming to controls at
159 37°C with matched population doublings. Among the 21,473 targeted genes, only one gene,
160 ribosomal protein S29 (Rps29)[25], was selectively required in control 37°C conditions and only nine
161 genes appeared selectively required during cold exposure (FDR < 0.1, log2 fold-change [Log2FC]
162 >1, **Figure 2b, Table S1, S2**). Four selectively required genes - *Dld*, *Lias*, *Lipt1*, and *Ybey* – are
163 involved in lipoylation and mitochondrial RNA processing[26–29]. Strikingly, five of the nine required
164 genes - *Gpx4*, *Eefsec*, *Pstk*, *Secisbp2*, and *Sepsecs* - represent known components of the
165 glutathione/Glutathione Peroxidase 4 (GPX4) antioxidant pathway, indicating that this pathway
166 functions as a potent suppressor of cold-induced cell death in hibernator-derived BHK-21 cells
167 (**Figure 2c**).
168
169 *Gpx4* encodes a selenocysteine-containing lipid antioxidant enzyme that acts to suppress lipid
170 peroxidation via the glutathione-mediated reduction of lipid hydroperoxides to non-toxic lipid

171 alcohols[30]. GPX4 inhibition sensitizes cells to ferroptosis, a distinct form of programmed cell death
172 characterized by iron-dependent accumulation of lipid peroxidation[31]. Notably, cold exposure has
173 previously been associated with increased lipid peroxidation and ferroptosis in human cells[5].
174 Underscoring the requirement for Gpx4 activity, four of the eight remaining genes selectively
175 required upon cold exposure (*Eefsec, Secisbp2, Pstk, Sepsecs*) are directly or indirectly involved
176 in selenocysteine incorporation into cellular proteins and thus required for Gpx4 activity (**Figures**
177 **2d-h**)[32,33].
178
179 Given that our initial screen design involved repeated rewarming cycles, we could not exclude the
180 possibility that the Gpx4 pathway confers resistance to rewarming-associated stress rather than
181 cold tolerance per se. To address this issue, we took advantage of the high cold tolerance of BHK-
182 21 cells and included a second screen arm using similar methods in which cells were continuously
183 exposed to 4°C for 15 days (**Figure 2i**). Sequencing prior to and following 15 days of cold
184 exposure, followed by a brief rewarming to 37°C, confirmed significant depletion (FDR < 0.1,
185 Log2FC < -0.5) of sgRNAs targeting *Gpx4*, *Eefsec*, and *Secisbp2* (as well as a trend toward
186 depletion for *Sepsecs* and *Pstk*), confirming a critical role for the Gpx4 pathway in BHK-21 cell
187 prolonged cold tolerance (**Figures 2j,k, Table S2, S3**). Thus, two unbiased genome-scale screen
188 arms identified Gpx4 as a major suppressor of cold-induced cell death in hibernator-derived BHK-
189 21 cells in the context of both cyclical and continuous cold exposure.
190
191 **Gpx4 catalytic activity is essential for hibernator cell survival during cold exposure**
192 To further validate the role of GPX4 in cold-mediated cell death, we employed the top-ranked
193 sgRNA from our screen to generate clonal *Gpx4* knockout BHK-21 cells. We sorted individual
194 cells to obtain clonal knockout cell lines and maintained them in the presence of liproxstatin-1
195 since they showed stunted growth at 37°C (**Figure S4a**). We confirmed the absence of Gpx4 via
196 immunoblotting (**Figure 3a**). While wild-type (WT) BHK-21 cells maintained high cell viability at
197 4°C, all three *Gpx4* knockout lines exhibited complete cell death within 4 days of cold exposure
198 (****$P < 0.0001$) (**Figure 3a)**. Moreover, these differences reflected Gpx4 loss, as opposed to
199 off-target effects insofar as lentiviral re-expression of cytosolic hamster Gpx4 (****$P < 0.0001$),
200 but not a GFP control gene or a catalytically dead mutant form of Gpx4 (mGPX4) that has a
201 serine in the active site instead of a selenocysteine, restored cold tolerance of *Gpx4* knockout
202 lines (**Figures 3b,c).**
203

204 Together, these genetic experiments strongly implicate the catalytic activity of Gpx4 in BHK-21
205 cold tolerance. However, the constitutive nature of these interventions precluded a determination
206 of whether Gpx4 functions to actively oppose cell death during cold-exposure or whether loss of
207 its catalytic activity prior to cold exposure sensitizes cells to subsequent cold challenge. To
208 address this issue, we used RSL3 and ML162, two competitive small-molecule Gpx4 inhibitors[34–
209 36]. Acute treatment of cultured BHK-21 cells with these inhibitors during cold exposure yielded
210 dose-dependent increases in cell death. Indeed, by four days of treatment, both RSL3- and
211 ML162-treated BHK-21 cells display significantly increased cold-induced death compared to
212 untreated controls (****$P < 0.0001$) (**Figures 3d,e**). Importantly, relative to WT cells, *Gpx4*
213 knockout cells exhibited no significant increase in cold-induced cell death upon RSL3 treatment
214 following a short cold exposure (8 hours) (**Figure S3**), confirming the specificity of these inhibitors
215 under the test conditions. We therefore conclude that Gpx4 catalytic activity is required in BHK-
216 21 cells during the course of cold exposure to actively oppose cold-induced cell death.
217
218 Given that Gpx4 activity acts as a major endogenous suppressor of ferroptosis[31], we tested
219 whether the cold-induced cell death observed under Gpx4 inhibition occurred via the ferroptosis
220 pathway. To this end, we made use of two small molecule inhibitors of ferroptosis, ferrostatin-1,
221 a lipophilic antioxidant, and deferoxamine mesylate (DFO), a Fe^{2+} chelator. Both inhibitors
222 effectively rescued cold-induced cell death in the presence of the Gpx4 inhibitor RSL3 (**Figure**
223 **3f**), indicating that acute inhibition of Gpx4 activity in the cold drives cell death via ferroptosis.
224 Together, through a combination of genetic and pharmacological approaches, our studies
225 demonstrate that Gpx4 activity confers substantial cold resistance in hibernator-derived cells,
226 protecting cells from cold-induced ferroptosis.
227
228 **Genome-scale CRISPR screen identifies determinants of cold sensitivity in human cells**
229 In contrast to hibernator-derived cell lines, human cells display varying cold sensitivities in
230 culture, with some exhibiting pronounced intolerance to the cold (**Figure 1d-g**). Consistent with
231 prior reports[5,8,37], pharmacological experiments in several human cell lines (K562, HT1080,
232 RPE, and HeLa cells) confirmed that cold-induced cell-loss occurred primarily via ferroptosis,
233 with both antioxidant ferroptosis inhibitors (ferrostatin-1 and liproxstatin-1) and iron chelators
234 (DFO and 2'2'-pyridine) increasing the cold survival in all four cell lines in a dose-dependent
235 manner. By contrast, neither the Caspase inhibitor Z-VAD-FMK nor the necroptosis inhibitor
236 necrostatin-1 significantly affected cell viability (**Figure S5, S6**).
237

238 To gain further insight into the genetic modifiers of human cell cold sensitivity and resistance,
239 we designed and performed an additional CRISPR-Cas9 screen in cold-sensitive human K562
240 cells exposed to cold temperatures. A pooled lentiviral CRISPR-Cas9 library targeting 19,381
241 genes (~5 sgRNAs per gene) was delivered to K562 cells at an MOI of ~0.5. Transduced cells
242 were placed at 4°C for five days to allow for cold-induced cell death to occur in approximately 79
243 ± 1.76% of cells, followed by a three-day rewarming to 37°C to allow for amplification of
244 remaining cells (**Figure 4a**). This cold-rewarming cycle was repeated three times, with cells
245 collected after each cycle to monitor the relative enrichment and depletion of individual sgRNAs.
246 As in our prior screens, separate cultures transduced in parallel were maintained at 37°C for
247 comparative analysis. In addition, to discriminate between ferroptosis-dependent and -
248 independent regulators of cold tolerance, we conducted a parallel screen in cold-exposed K562
249 cells under continuous ferrostatin-1 treatment. As before, the efficiency and specificity of the
250 screens were assessed based on effective depletion of characterized core essential genes[24] as
251 well as the lack of depletion of negative control guides (250 nontargeting and 125 intergenic
252 sgRNAs) (**Figure S7)**.
253
254 To our surprise, this screen did not identify any genes whose disruption significantly enhanced
255 K562 cold tolerance. By contrast, we identified 176 genes selectively required during cold
256 cycling relative to constant 37°C control conditions (FDR < 0.1, LFC < -0.1, and requiring >2
257 sgRNAs, **Figure 4b**). It is notable that K562 cold survival was sensitive to the targeting of larger
258 number of genes than the BHK-21 line, potentially indicating increased dependencies on
259 genetic pathways which are not essential in BHK-21 cells (**Figure S8, Table S6**). Among the
260 pathways identified, we honed in on the selenocysteine incorporation pathway and observed
261 *GPX4* and the selenocysteine incorporation genes *PSTK*, *SEPSECS*, and *EEFSEC* within the
262 top-ranked K562 cold-protective genes, suggesting that the GPX4 pathway confers significant
263 resistance to the cold not only in cold-tolerant hibernator cells, but also in cold-sensitive human
264 cells (**Figures 4c-g**). Notably, we identified 11 genes that were no longer essential (Fold
265 enrichment > 0.50, FDR < 0.10) in the presence of Ferrostatin-1, indicating that these genes act
266 to suppress cold-induced ferroptosis (**Figures 4h-n, Table S4, S5**). Although multiple pathways
267 have been described as suppressors of ferroptosis in other contexts[38–42], it is notable that 5 of
268 11 identified genes represent known components of the GPX4 pathway.
269
270 To confirm these findings, we generated three clonal *GPX4* knockout K562 cell lines and
271 confirmed the loss of GPX4 via immunoblotting (**Figure 5a**). Similar to our findings in BHK-21

272 cells, K562 *GPX4* knockout clones exhibited stunted growth and were expanded in the
273 presence of liproxstatin-1 (**Figure S4b**). Importantly, GPX4 loss greatly increased cold-induced
274 cell death (****$P < 0.0001$) (**Figures 5a**), thus confirming an essential role for *GPX4* in human
275 cell cold tolerance. Similar effects were also observed upon acute pharmacologically inhibition
276 of GPX4 with RSL3 or ML162 at 4°C (****$P < 0.0001$) (**Figures 5b, c**). These effects were
277 dependent on GPX4 inhibition insofar as the cold tolerance of K562 *GPX4* knockout cells was
278 unaffected by RSL3 treatment (**Figure S9**). In addition, RSL3-driven cold-induced cell death
279 was rescued by either ferrostatin-1 or DFO treatment, indicating that RSL3-induced cell loss
280 occurs via the ferroptosis pathway (**Figure 5d**). Increased cold-induced death in the *GPX4*
281 knockout K562 cell lines could be rescued upon lentiviral expression of either the cytosolic
282 human (hs) or hamster (ma) GPX4, but not GFP or catalytically dead GPX4 variants (**Figure**
283 **5e).** Together, our genetic and pharmacological studies reveal that K562 cells, despite being
284 significantly less cold-tolerant than hamster BHK-21 cells, also rely on the GPX4 pathway to
285 suppress cold-induced ferroptosis.
286
287 **GPX4 catalytic activity is limiting for K562 cell cold tolerance**
288 Given that the GPX4 pathway is active during cold exposure and essential for cold survival in
289 both hamster BHK-21 and human K562 cells, it is somewhat surprising that these cell lines
290 exhibit markedly different cold tolerances. In this regard, it has previously been suggested[5] that
291 upon cold exposure human cells, in contrast to hibernator-derived cells, rapidly deplete
292 intracellular glutathione, an essential co-factor for GPX4 function, which could thus account for
293 their increased cold sensitivity. To test this idea, we supplemented K562 growth media with
294 either cell-permeable Glutathione reduced ethyl ester (GSH-MEE), N-acetyl-cysteine (NAC), or
295 L-Cystine, a glutathione precursor; however, these interventions failed to significantly increase
296 K562 cells' cold tolerance under our culture conditions (**Figure S10**). We therefore examined
297 the possibility that GPX4 protein levels in K562 cells are limiting for their cold tolerance. To this
298 end, we generated K562 lines overexpressing either human or hamster GPX4. Both of these
299 overexpression lines exhibited strikingly improved cold tolerance compared to the wild-type
300 K562 parental line and a GFP-overexpressing control cell line (****$P < 0.0001$) (**Figure 5f**.
301 Indeed, GPX4-overexpressing K562 cells displayed comparable cold tolerance to that of
302 hibernator-derived BHK-21 cells (**Figure 1d, g**). To confirm that increased GPX4 catalytic
303 activity was responsible for the improved cell cold tolerance, we generated additional K562 lines
304 overexpressing catalytically dead forms of hamster or human GPX4 in which the active site
305 selenocysteine was mutated to serine and found that these GPX4 mutant lines exhibited no

306 increase in cold tolerance (**Figure 5f**). Taken together, these results strongly suggest that GPX4
307 abundance serve as a key limiting determinant of K562 cell cold tolerance. Moreover, our
308 finding that human and hamster GPX4 overexpression confer comparable increases in K562
309 cold tolerance may indicate that the intrinsic activity of the hamster and human GPX4 enzymes
310 are similar.
311
312 **GPX4 activity is broadly required for cold tolerance in primary cells across evolutionarily**
313 **distant mammalian species**
314 Given that our studies had largely employed a small number of transformed cell lines, we
315 sought to extend our investigation to examine cold tolerance in primary cell types as well as
316 cells derived from additional hibernating species. To this end, we obtained primary and
317 immortalized fibroblasts from human, mouse, and rat as well as from Syrian hamster, 13-lined
318 ground squirrel (*Ictidomys tridecemlineatus*), and horseshoe bat (*Rhinolophus ferrumequinum*),
319 three distantly related mammalian hibernators, and characterized their cold tolerance. While
320 hibernator-derived fibroblasts exhibited robust, roughly uniform cold tolerance, we observed a
321 surprisingly variable degree of cold tolerance across non-hibernator primary cells (**Figure 6a**),
322 with human dermal fibroblasts exhibiting a remarkable 79 ± 4.93% cell viability after seven days
323 at 4ºC, comparable to that observed with hamster-derived BHK-21 cells.
324
325 To examine the role of GPX4 in primary cell cold resistance, we transduced cells with Cas9 and
326 sgRNAs targeting human *GPX4* to create a population of *GPX4* knockout human kidney
327 fibroblasts (**Figure 6b**). Consistent with our prior findings in cell lines, GPX4 loss resulted in
328 significantly decreased viability in the cold, which was largely rescued by ferrostatin-1 treatment
329 in fibroblast cells (**Figure 6b**). Indeed, RSL3 treatment significantly decreased the viability of
330 wild-type cold-exposed human kidney fibroblasts **(Figures 6c, d)**, and these effects were
331 dependent on GPX4 inhibition as the cold tolerance of human kidney fibroblast *GPX4* knockout
332 cells was largely unaffected by RSL3 treatment (**Figure S4c**).
333
334 To more widely examine the dependence of primary cell cold tolerance on GPX4 activity, we
335 obtained and tested fibroblasts derived from six mammalian species. We found the GPX4
336 activity widely contributes to cold tolerance across hibernators and non-hibernators was
337 dependent on GPX4, as RSL3-treated cells showed increased cold-induced cell death that was
338 largely rescued by ferrostatin-1 treatment (**Figures 6e, f**). We also extended these findings to a
339 non-fibroblast cell type, obtaining similar results with primary cortical neuronal cultures prepared

340 from neonatal mice and hamsters (**Figures 6g, h**). Taken together, our data indicate that
341 primary cell types are strongly sensitive to GPX4 loss in the cold and suggest that their
342 differential cold sensitivities may reflect different levels of GPX4-mediated cold tolerance.
343
344 **Discussion**
345 Hibernators can lower their body temperature to ~4°C for several days to weeks, indicating that
346 their cells and tissues possess the ability to survive extended periods of cold. Previous studies
347 have indicated that ferroptosis contributes to cold-induced cell death in cultured human
348 cells[5,8,37]; however, the genetic modifiers of cold sensitivity in hibernators and non-hibernators
349 have yet to be systematically explored. Here, we conducted a series of unbiased genome-wide
350 CRISPR-Cas9 screens in both hibernator- and non-hibernator-derived cells to investigate the
351 mechanisms controlling cellular cold tolerance. Our findings, further validated using stable
352 genetic knockout lines and pharmacological inhibitors, identify the GPX4 pathway as a critical
353 suppressor of cold-induced cell death. Indeed, overexpression studies in human K562 cells
354 suggest that GPX4 abundance can serve as a key limiting determinant of cellular cold tolerance.
355 Notably, Sone et al.[43] recently also identified GPX4 as a strong regulator of cold tolerance
356 through overexpression screening. These independent findings further support the current study
357 identifying GPX4 as a conserved suppressor of cold-induced cell death. The consistency of our
358 observations across diverse cell lines and primary cells, including cells derived from six different
359 mammalian species, argues that GPX4 serves as an essential and evolutionarily conserved
360 mechanism to protect cells from cold-induced ferroptotic cell death.
361
362 During the course of our studies, we made the surprising observation that cells stained with the
363 commonly employed membrane-impermeable dye trypan blue exhibit increased dye retention
364 immediately after cold exposure, an artifact not reflecting genuine cell death. Rather, cell
365 counting following brief rewarming yields more accurate results, in some cases reflecting
366 significantly higher cell viability than previously appreciated. Employing this modified approach
367 to measure cold-induced cell death across sixteen cell lines and primary cell types points to
368 more nuanced variations in cold survival across cell types. These differences are highlighted by
369 the pronounced contrast between the poor cold viability of human HT1080 cells and the robust
370 cold tolerance observed in human fibroblasts. The underlying basis of this transient cell
371 permeability for trypan blue following cold exposure remains unclear; however, it is noteworthy
372 that in *S. cerevisiae* heat and chemical insults have been found to induce a brief window of
373 membrane permeability to PI prior to membrane repair[44]. Likewise, uptake of propidium ions

374 across intact cell membranes has been previously observed in bacteria showing high
375 membrane potentials[45]. Our observations suggest that further investigation into the mechanisms
376 underlying transient membrane permeability in different cell types and stress conditions could
377 lead to improved methods for accurately measuring cell viability, ultimately enhancing our
378 understanding of cellular stress.
379
380 We report, to our knowledge, the first genome-scale hibernator CRISPR-Cas9 screen in cells
381 derived from Syrian hamster. To create a genome-scale CRISPR-Cas9 library, we implemented
382 a CRISPOR-based computational pipeline for sgRNA selection and benchmarked its success
383 by carrying out the hamster and human screens described here. Our validated sgRNA libraries
384 and associated algorithms should serve as a valuable resource to the hibernation community,
385 as well as other scientific communities developing CRISPR-based tools for non-model
386 organisms.
387
388 While our data point to GPX4 levels as a major determinant of cellular cold tolerance, whether
389 endogenous levels of functional Gpx4 across various cell types correlates with their cold
390 tolerance remains to be tested. It also remains possible that other factors such as GPX4
391 subcellular localization, the abundance of the cellular selenocysteine incorporation machinery,
392 the abundance of glutathione, as well as GPX4-pathway independent factors all play important
393 roles in limiting cold tolerance across various cell types. Although we did not see an increase in
394 cold cell viability upon treatment of K562 cells with GSH-MEE, it is notable that in our screens,
395 sgRNAs targeting genes involved in the glutathione biosynthesis (e.g. *GCLC*, *GSS*[46,47]) showed
396 increased depletion in cold-exposed K562 versus BHK-21 cells (**Figure S10, Figure S11**). This
397 suggest a reduced dependency on the conventional glutathione biosynthetic pathway in cold-
398 exposed BHK-21 cells. In addition, while our data points to a key cellular need to reduce cold-
399 associated lipid hydroperoxides, the mechanisms that drive peroxide accumulation in the cold
400 remain unclear. Specifically, the roles of reactive oxygen species (ROS) production,
401 polyunsaturated fatty acid (PUFA) levels, and free iron concentration should be further explored
402 to understand the specific drivers of cold-induced ferroptotic cell death. Such insights have the
403 potential to inform the development of more effective strategies for managing conditions
404 exacerbated by cold exposure, such as ischemic injuries and organ transplantation.
405
406 We limited our current investigations to cell culture paradigms. However, future *in vivo* studies in
407 hibernating organisms that naturally undergo profound drops in core body temperature could

yield further insight into the adaptive mechanisms that govern cellular survival during periods of hibernation and torpor, while also allowing for the study of cold tolerance mechanisms in cell types that cannot presently be maintained in culture. Similarly, a *Gpx4* conditional knockout mouse line has been generated and used to show that *Gpx4* is essential for mitochondrial integrity and neuronal survival in adult animals[48]; however, these animals have not yet been used to evaluate the contribution of *Gpx4* to *in vivo* cellular and tissue cold tolerance.

The ability to hibernate and survive long-term cold exposure is present in many mammalian species from rodents to bats to primates, raising the possibility that the ability to enter hibernation and tolerate cold was an ancestral trait present in protoendotherms. Our observation that a single pathway centered around GPX4 is required across diverse mammalian species to protect cells from cold-induced cell death, raises a question whether GPX4 has a role in protection from cold-induced ferroptosis in other cold-tolerant vertebrates including fish, amphibians, reptiles, and birds that also enter torpor. Such studies will advance our understanding of the evolved mechanisms by which cells mitigate cold-associated damage—one of the most common challenges faced by cells and organisms in nature.

Acknowledgments

We thank Wei Li for generously sharing 13-lined ground squirrel (*Ictidomys tridecemlineatus*) fibroblasts and Thomas P. Zwaka for sharing greater horseshoe bat (*Rhinolophus ferrumequinum*) fibroblasts. We thank Amanda Chilaka and Sumeet Gupta of the Whitehead Institute Genome Technology Core for high-throughput sequencing. We thank Aurora Lavin-Peter, Aleksandar Markovski, Tara Thakurta, William S. Owens, Sheamin Khyeam, Karina Smolyar, and Elena Assad for their technical support. We thank Whitney Henry, Matthew Vander Heiden, Alison Ringel, Morgan Sheng, Myriam Heiman, and members of the Hrvatin laboratory for providing feedback on the study. Schematics created with BioRender.com. This material is based upon work supported by the National Science Foundation Graduate Research Fellowship under Grant No. 2141064 and The Paul and Daisy Soros Fellowship for New Americans (PSM). Research reported in this publication was supported by The G. Harold and Leila Y. Mathers Charitable Foundation and the NIDDK/NIH under Award Number DP2DK136123. The content is solely the responsibility of the authors and does not necessarily represent the official views of the National Institutes of Health.

Author contributions

B.L., K.M.K., and S.H. conceived and designed the study. B.L. and K.M.K. designed, performed, and analyzed experiments. B.L., K.M.K., H.R.K. designed and performed genome wide CRISPR screens. A.K. assisted with the genome wide CRISPR screens. B.L. performed the genetic and pharmacological studies to validate the screens. K.M.K. performed the experiments with primary cells. E.M.F. and G.W.B. designed algorithms to select genome-wide Syrian hamster (*Mesocricetus auratus*) CRISPR library. M.E.B. and P.B. immortalized mouse embryonic fibroblasts and greater horseshoe bat (*Rhinolophus ferrumequinum*) fibroblasts. J.M.R., R.J., J.S.W., and E.C.G. advised on the study. B.L., S.H., and E.C.G led the writing of the manuscript with contributions from other authors. E.C.G. and S.H. obtained funding for the research. All authors approved and reviewed the manuscript.

Declaration of interests

The authors declare no competing interests.

Figures

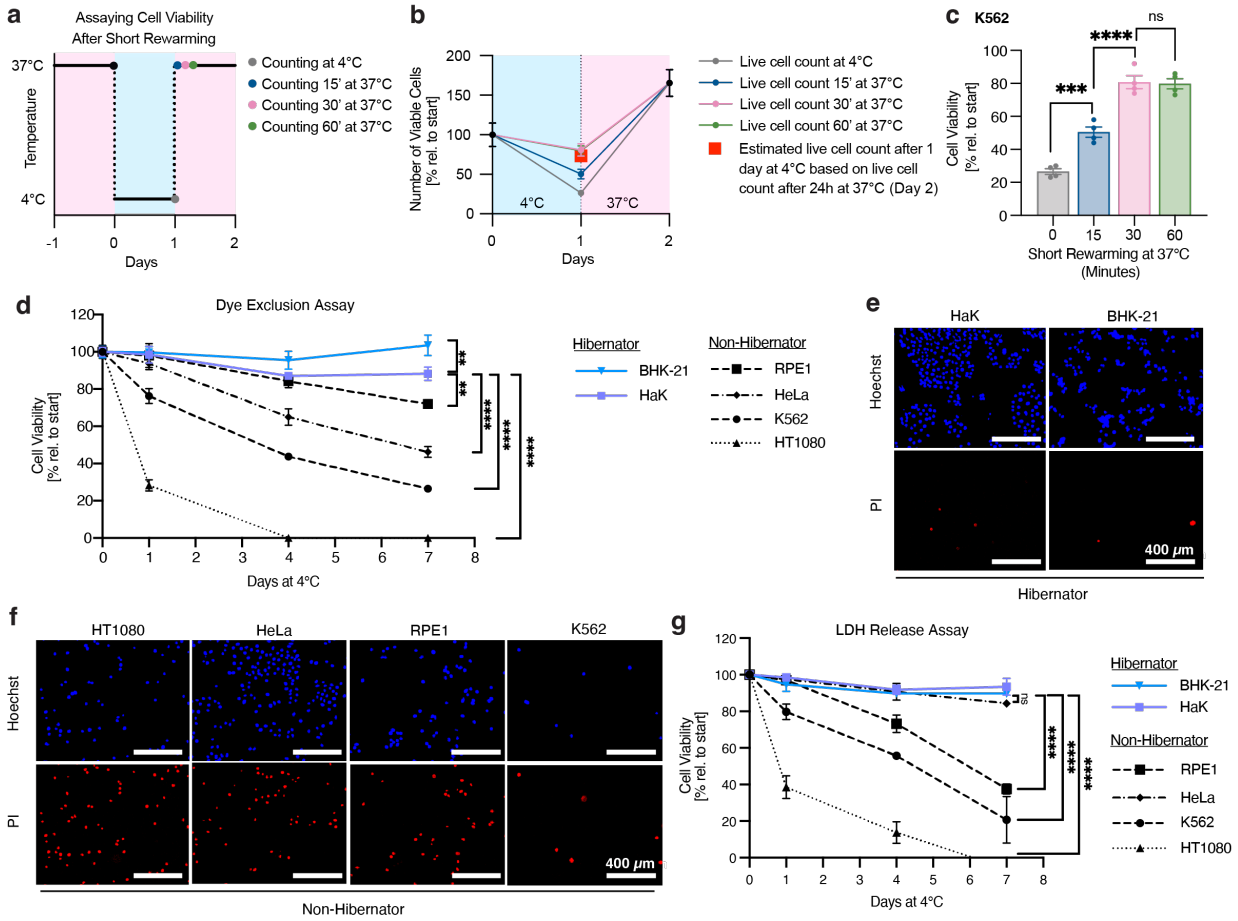

Figure 1. Hibernator-derived cells exhibit increased cold resistance

a, Schematic of cold cell viability counting, consisting of 1 day cold exposure (4°C), followed by a short rewarming at 37°C for 15, 30, or 60 minutes before trypan blue staining. **b,** Number of viable K562 cells based on trypan blue staining after one day at 4°C and subsequent rewarming for 24 hours at 37°C. Numbers are normalized to initial cell counts. Blue shaded regions indicate 4°C exposure and shaded pink regions indicate 37°C exposure. Red square indicates calculated cell counts after one day at 4°C based on the viable cell number measured after 24 hour rewarming. **c**, Viability of K562 cells was assessed by trypan blue staining after incubation at 37°C for 0, 15, 30, or 60 minutes following 24 hours at 4°C (n = 4). Cells incubated at 37°C for 15, 30, and 60 minutes show a significant increase in cell counts compared to cells counted

492 without rewarming (n = 4 samples per condition, ***P = 0.0007, ****P < 0.0001). **d**, Viability of
493 hibernator (BHK-21, HaK)- and non-hibernator (HeLa, RPE1, HT1080, K562)-derived cell lines
494 at 4°C as measured by trypan blue staining. Hibernator-derived lines show significantly
495 increased cold resistance compared to lines derived from non-hibernators at 7 days 4°C (n = 4
496 samples per data point, ****P < 0.0001). **e, f**, Fluorescence images of hibernator- and non-
497 hibernator-derived cell lines after 4 days at 4°C. Cultures were stained with 1 µg/mL Hoechst
498 33342 and 1 µg/mL propidium iodide (PI) to distinguish live and dead cells. **g**, Viability of
499 hibernator- and non-hibernator-derived cell lines at 4°C as measured by LDH release (n = 4
500 samples per data point, ****P < 0.0001). All values show mean ± SEM, with significance
501 measured by one-way ANOVA adjusted for multiple comparisons by Dunnett's test. *P < 0.05;
502 **P < 0.01; ***P < 0.001; ****P < 0.0001; ns P > 0.05.
503
504
505

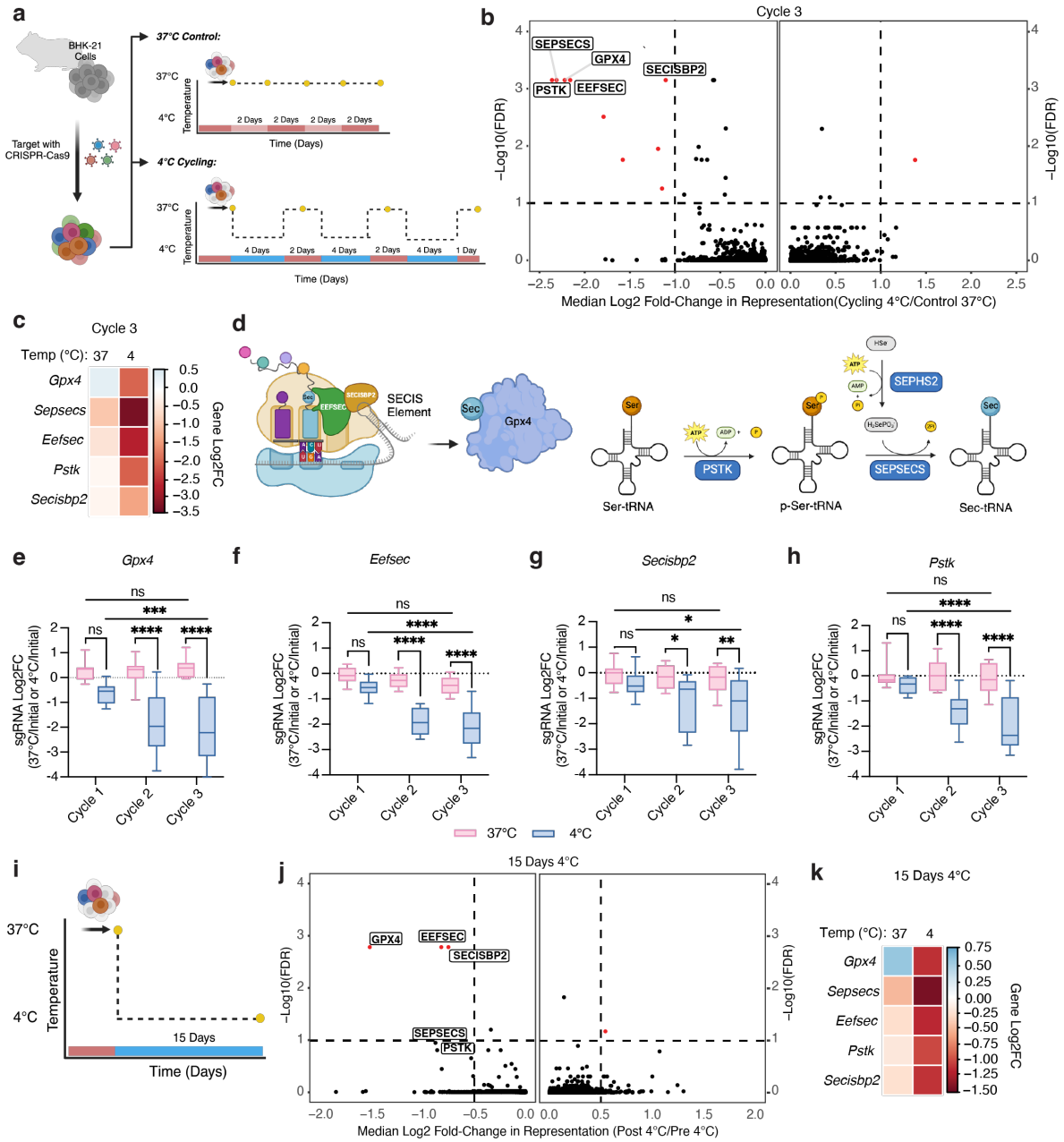

Figure 2. Unbiased CRISPR screens identify the GPX4 pathway as necessary for cold-induced survival in hibernator-derived BHK-21 cells

a, Schematic of CRISPR screen paradigm, consisting of four passages of control cells kept at 37°C and three cycles of cold exposure (4°C) for 4 days followed by rewarming (37°C) for 2 days. Yellow dots indicate points of sample collection. **b**, Volcano plot showing median log2 fold-change of genes after three cycles of cold exposure and rewarming (4°C) compared to cells following three passages at 37°C. Red dots indicate selectively required genes with a median log2 fold-change < -1 or > 1 and FDR < 0.1. **c**, Heatmap of the median log2FC of ferroptosis-

515 related genes after three cycles of cold exposure and rewarming (4°C) compared to three
516 passages at 37°C. **d**, Partial schematic of the selenocysteine incorporation pathway. Left:
517 Production of the GPX4 selenoprotein requires recoding of a UGA codon to the amino acid
518 selenocysteine (Sec). This process involves a cis-acting SECIS element within the *Gpx4* mRNA
519 3' UTR, SECIS binding protein 2 (SECISBP2), a specific eukaryotic elongation factor
520 (EEFSEC), and Sec-charged tRNA. Right: The Sec-charged tRNA is generated by the
521 combined action of Phosphoseryl-tRNA kinase (PSTK), Selenophosphate synthetase 2
522 (SEPHS2), and selenocysteine synthase (SEPSECS). **e-h**, Median log2 fold-change (log2FC) of
523 10 guides per targeted gene, showing guide depletion over three cycles of cold exposure and
524 rewarming. Significance between Cycle 1 versus Cycle 3 is measured by two-way ANOVA
525 adjusted for multiple comparisons by Dunnett's test. Significance between 37°C and 4°C for
526 each cycle is measured by two-way ANOVA adjusted for multiple comparisons by Bonferroni's
527 test. **e**, *Gpx4*, **f**, *Eefsec*, **g**, *Secisbp2,* **h**, *Pstk*. **i**, Schematic of CRISPR screen paradigm,
528 showing cells exposed to 4°C continuously for 15 days. Yellow dot indicates point of sample
529 collection. **j**, Volcano plot showing median log2 fold-change in abundance of guides targeting
530 the indicated genes after 15 days of 4°C exposure compared to one passage at 37°C. Red dots
531 indicate selectively required genes with a median log2 fold-change < -0.5 or > 0.5 and FDR <
532 0.10. **k**, Heatmap of the median log2FC in abundance of guides targeting ferroptosis-related
533 genes after 15 days of 4°C exposure compared to 37°C control cultures. *$P < 0.05$; **$P < 0.01$;
534 ***$P < 0.001$; ****$P < 0.0001$; ns $P > 0.05$.
535

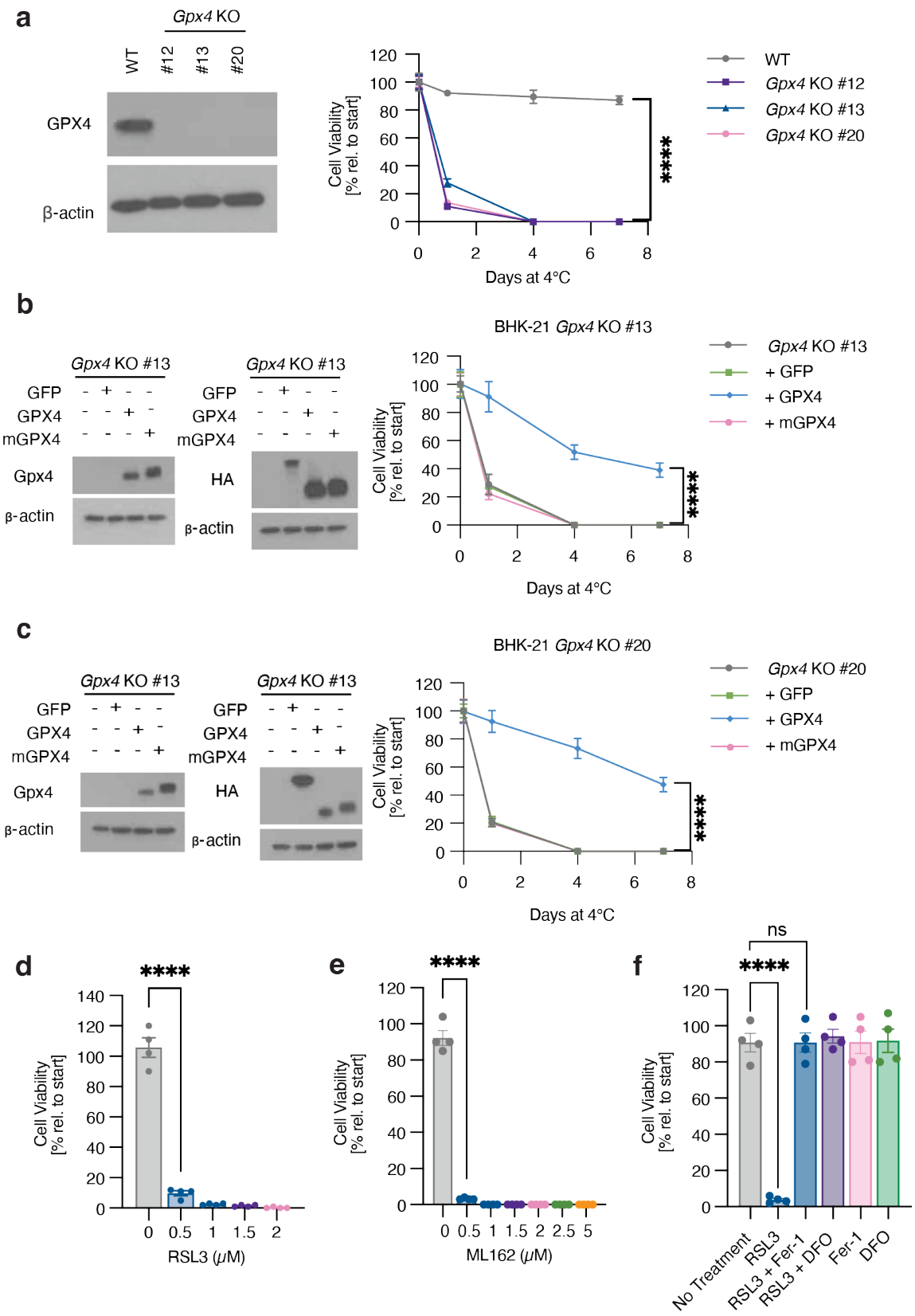
a
Gpx4 KO
WT
#12
#13
#20
GPX4
β-actin
Cell Viability [% rel. to start]
Days at 4°C
WT
Gpx4 KO #12
Gpx4 KO #13
Gpx4 KO #20
****
b
Gpx4 KO #13
GFP
GPX4
mGPX4
Gpx4
HA
β-actin
BHK-21 Gpx4 KO #13
+ GFP
+ GPX4
+ mGPX4
c
BHK-21 Gpx4 KO #20
Gpx4 KO #20
d
RSL3 (μM)
e
ML162 (μM)
f
ns
No Treatment
RSL3
RSL3 + Fer-1
RSL3 + DFO
Fer-1
DFO

536

537

538 **Figure 3. GPX4 activity is required for BHK-21 cell cold tolerance**

539 **a**, Stable *Gpx4* knockout (KO) BHK-21 cell lines exhibit reduced cold tolerance. Left: Western
540 blot of wild-type (WT) and individual *Gpx4* KO clone lysates for GPX4 and β-actin loading
541 control. Right: Viability of *Gpx4* KO lines is significantly lower than WT BHK-21 cells at 7 days
542 4°C by trypan blue staining (n = 4, ****P < 0.0001), with complete cell death by four days at 4°C.
543 **b, c**, Reintroduction of wild-type Syrian hamster GPX4 (GPX4), but not a catalytically dead form
544 of GPX4 (mGPX4) rescues cold-induced cell death in two independent BHK-21 *Gpx4* KO clonal
545 cell lines. Left panels: Western blots for HA and GPX4 along with β-actin loading control. Right
546 panels: Expression of WT hamster GPX4 showed significantly higher cell viability at 7 days 4°C
547 compared to the corresponding parental *Gpx4* KO, GFP-, and mGPX4-expressing lines by
548 trypan blue staining (n = 4, ****P < 0.0001). **d, e**, Treatment with the GPX4 inhibitors RSL3 (**d**)
549 or ML162 (**e**) results in enhanced cold-induced death in BHK-21 cells by 4 days at 4°C as
550 measured by trypan blue exclusion (n = 4, ****P < 0.0001). **f**, Cold-induced BHK-21 cell death
551 upon RSL3 treatment occurs via ferroptosis. BHK-21 cells were placed at 4°C and treated with
552 RSL3 (1 μM) and/or the ferroptosis inhibitor ferrostatin-1 (Fer-1, 1 μM) or iron chelator DFO
553 (100 μM) for 4 days (n = 4). Treatment with RSL3 resulted in significantly lower cell viability than
554 no treatment as determined by one-way ANOVA adjusted for multiple comparisons by Tukey's
555 HSD (****P < 0.0001). All values show mean ± SEM, with significance measured by two-tailed t
556 test, unless otherwise indicated. *P < 0.05; **P < 0.01; ***P < 0.001; ****P < 0.0001; ns P >
557 0.05.

558

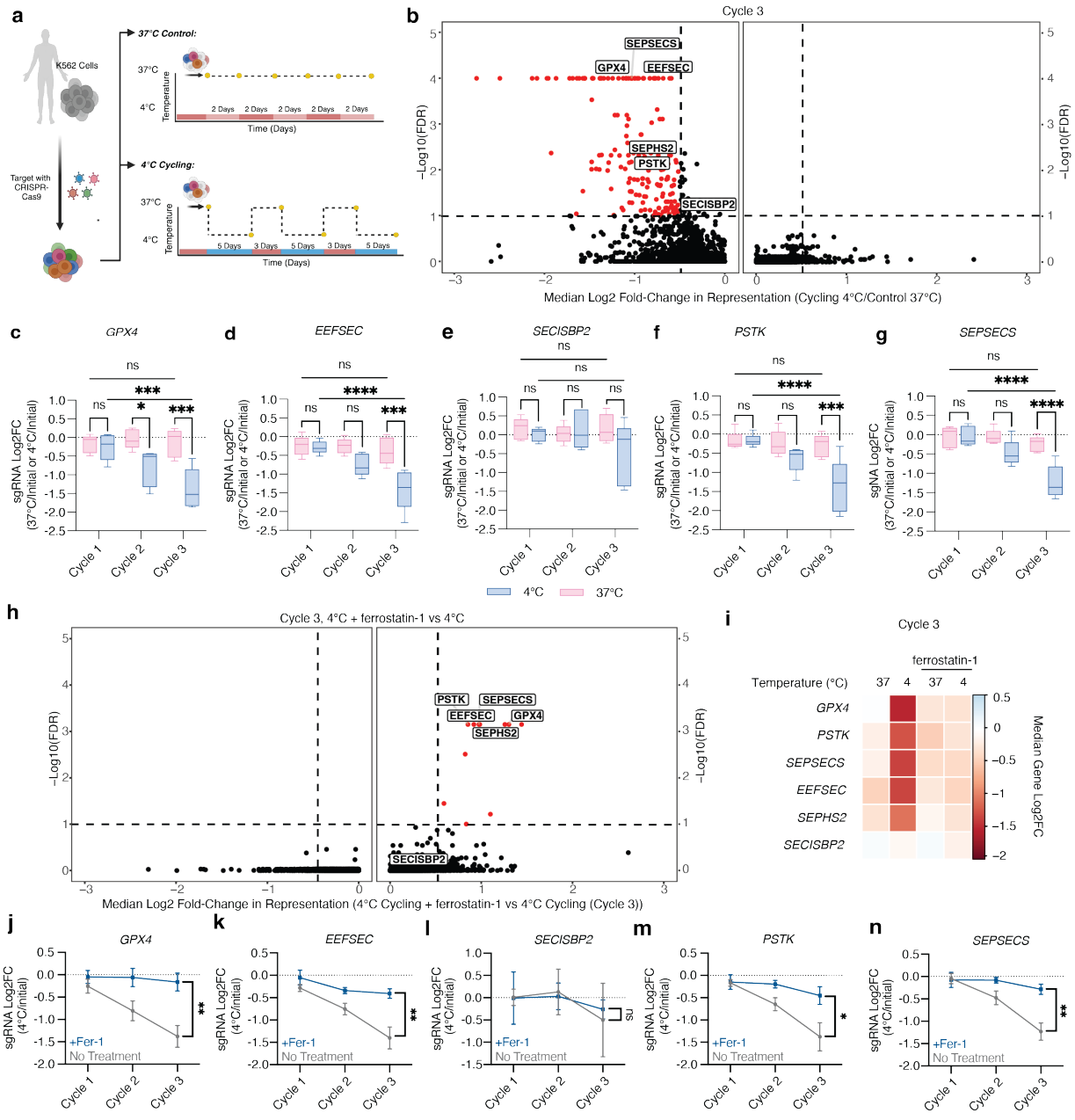

Figure 4. Genome-wide CRISPR screens identify GPX4 as a suppressor of cold-induced cell death in human cells

a, Schematic of CRISPR screen paradigm, consisting of three cycles of 5 days of cold exposure (4°C) interrupted by 3 day rewarming (37°C) periods. Yellow dots indicate points of sample collection. **b**, Volcano plot showing median log2 fold-change in abundance of guides targeting the indicated genes after three cycles of 4°C cold exposure compared to three passages at 37°C (Control). Red dots indicate selectively required genes with a median log2 fold-change < -

568 0.5 or > 0.5 and FDR < 0.1. **c-g**, Combined median log2 fold-change (log2FC) of 5 sgRNAs per
569 targeted gene, showing sgRNA depletion over three cycles of cold exposure. Significance
570 between Cycle 1 versus Cycle 3 is measured by two-way ANOVA adjusted for multiple
571 comparisons by Dunnett's test. Significance between 37°C and 4°C for each cycle is measured
572 by two-way ANOVA adjusted for multiple comparisons by Bonferroni's test. **c**, *GPX4*, **d**,
573 *EEFSEC*, **e**, *SECISBP2*, **f**, *PSTK*, **g**, *SEPSECS*. **h**, Volcano plot showing median log2 fold-
574 change in abundance of guides targeting the indicated genes after three cycles of 4°C cold
575 exposure in the presence or absence of 1 μM of ferrostatin-1. Red dots indicates selectively
576 required genes with a log2 fold-change < -0.5 or > 0.5 and FDR < 0.1. **i**, Heatmap of the median
577 log2FC in abundance of guides targeting ferroptosis-related genes after three cycles of cold
578 exposure (4°C) compared to 37°C control cultures with and without ferrostatin-1. **j-n**, Depletion
579 of 5 sgRNAs per gene over three cycles of cold exposure and rewarming with and without
580 ferrostatin-1 (1 uM) treatment. **j**, *GPX4* (***P* = 0.0047), **k**, *EEFSEC* (***P* = 0.0059), **l**, *SECISBP2*
581 (ns, *P* = 0.5457), **m**, *PSTK* (**P* = 0.0393), **n**, *SEPSECS* (***P* = 0.0029) as measured by two-
582 tailed t-test at Cycle 3. All values show mean ± SEM. **P* < 0.05; ***P* < 0.01; ****P* < 0.001; *****P*
583 < 0.0001; ns *P* > 0.05.
584

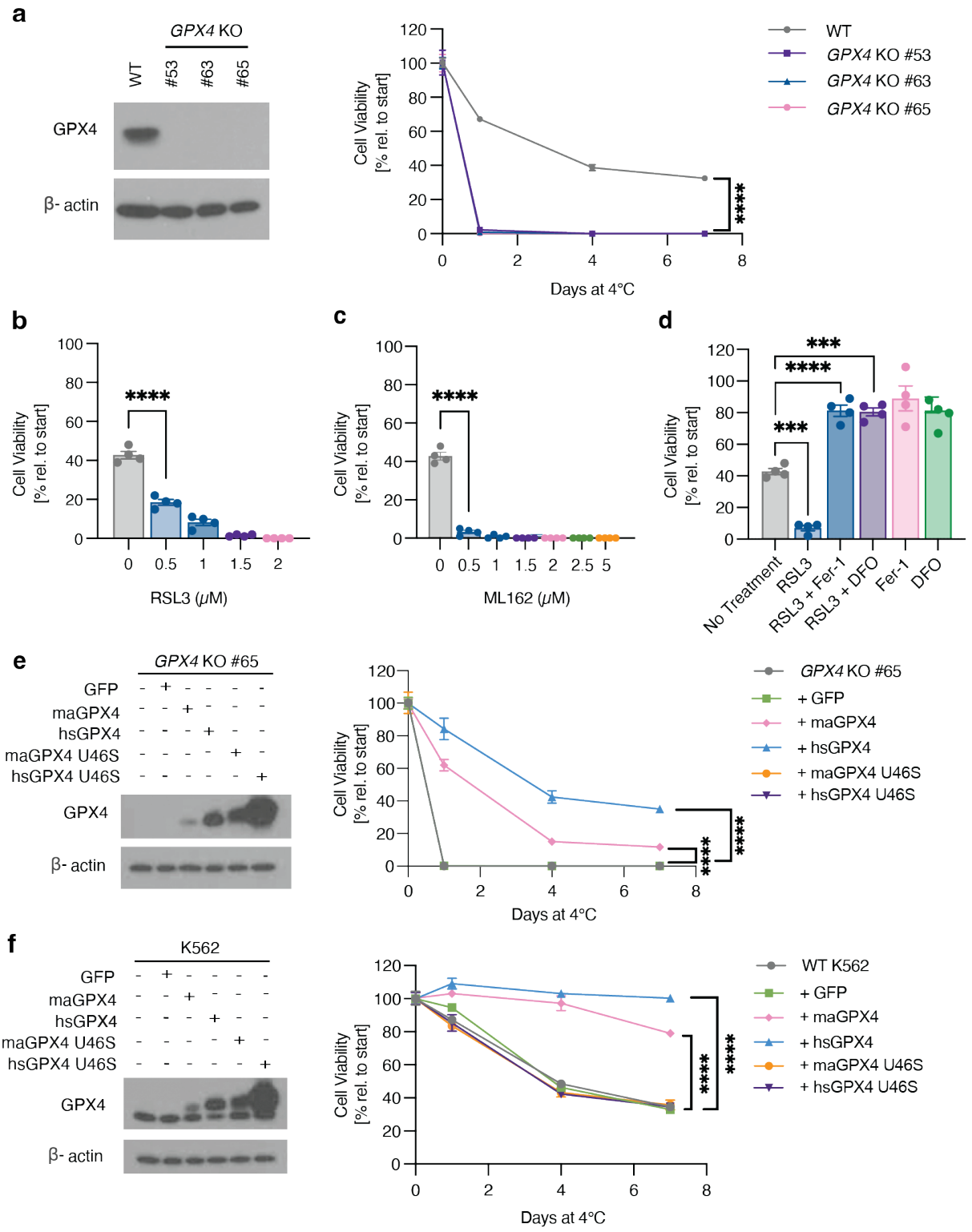

Figure 5. Endogenous GPX4 activity is limiting for K562 cell cold tolerance

a, Stable *GPX4* knockout (KO) K562 cell lines exhibit reduced cold tolerance. Left: Western blotting of wild-type (WT) and individual *GPX4* KO clones for GPX4 and β-actin loading control. Right: Viability of *GPX4* KO lines is significantly lower than WT K562 cells as measured by trypan blue staining ($n = 4$, ****$P < 0.0001$), with complete cell death by one day at 4°C. Significance measured by two-tail t-test at 7 days 4°C. **b, c**, Treatment with the GPX4 inhibitors RSL3 (**b**) or ML162 (**c**) results in enhanced K562 cold-induced death by 4 days at 4°C ($n = 4$, ****$P < 0.0001$) as measured by two-tailed t-test. **d**, Cold- and RSL3-induced K562 cell death occurs via ferroptosis. K562 cells were placed at 4°C and treated with RSL3 (1 μM) and/or the ferroptosis inhibitor ferrostatin-1 (Fer-1, 1 μM) or iron chelator DFO (5 μM) for 4 days ($n = 4$). Treatment with RSL3 resulted in significantly lower cell viability than no treatment as determined by one-way ANOVA adjusted for multiple comparisons by Tukey's HSD (***$P = 0.0002$). **e**, Reintroduction of wild-type human (hs) or hamster (ma) GPX4, but not catalytically dead forms of GPX4 (Gpx4 U46S), rescues cold-induced cell death in a K562 *GPX4* KO clonal cell line ($n = 4$). Left: Western blot for GPX4 levels and β-actin loading control. Right: Expression of WT human GPX4 and hamster GPX4 resulted in significantly higher cell viability compared to the corresponding parental *GPX4* KO, GFP-, and mutGPX4-expressing lines by trypan blue staining, as measured by one-way ANOVA adjusted for multiple comparisons by Dunnett's test at 7 days 4°C (****$P < 0.0001$). **f**, Overexpression of wild-type human or hamster GPX4, but not catalytically dead forms of GPX4 (mutGPX4), suppresses cold-induced cell death in a K562 cells (n = 4). Left: Western blot for GPX4, with β-actin loading control. Right: Expression of WT human GPX4 and hamster GPX4 resulted in significantly higher cell viability compared to wild-type, GFP-, and mutGPX4-expressing K562 lines by trypan blue staining, as measured by one-way ANOVA adjusted for multiple comparisons by Dunnett's test at 7 days 4°C (****$P < 0.0001$). All values show mean ± SEM. *$P < 0.05$; **$P < 0.01$; ***$P < 0.001$; ****$P < 0.0001$; ns $P > 0.05$.

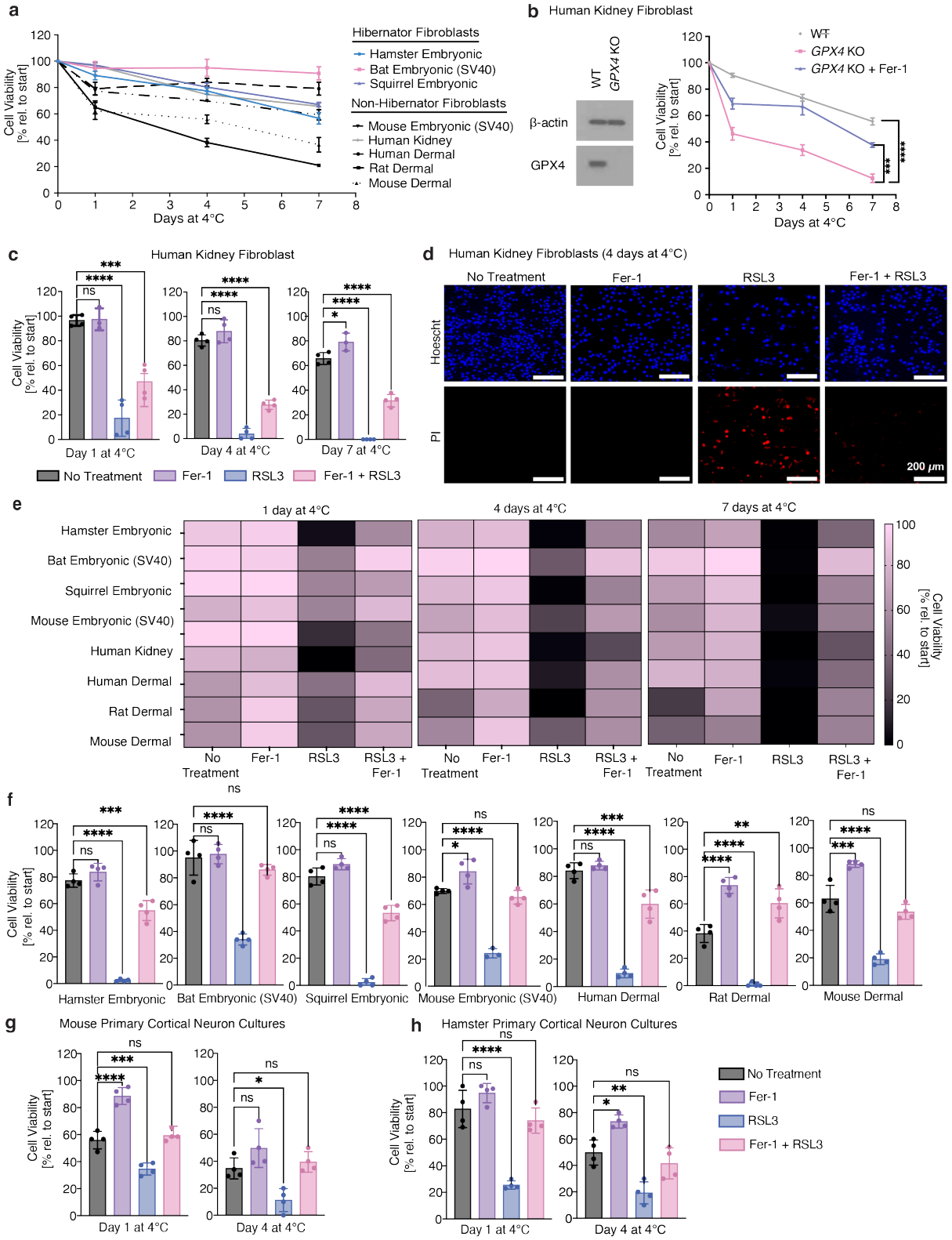

Figure 6. GPX4 is required for cold tolerance across both several hibernator and non-hibernator mammalian species and cell types

617 **a**, Viability of hibernator cells (Syrian hamster embryonic fibroblasts, Greater horseshoe bat
618 embryonic fibroblasts, and 13-lined ground squirrel embryonic fibroblasts) and non-hibernator
619 cells (SV40-immortalized mouse embryonic fibroblasts, human adult kidney fibroblasts, human
620 adult dermal fibroblasts, rat adult dermal fibroblasts, and mouse adult dermal fibroblasts)
621 exposed to 4°C as measured by trypan blue staining (n = 4, ****$P < 0.0001$). **b**, Human kidney
622 fibroblast *GPX4* knockout cells exhibit reduced cold tolerance compared to WT cells. Left:
623 Western blot of wild-type (WT) and *GPX4* KO cells for GPX4 and β-actin loading control. Right:
624 Viability of *GPX4* KO cells is significantly lower than WT cells at 4°C as measured by trypan
625 blue staining (n = 4, ****$P < 0.0001$). **c**, Gpx4 activity is essential for cold survival of primary
626 human kidney fibroblasts. Human kidney fibroblasts were placed at 4°C and left untreated or
627 treated with RSL3 (1 μM) and/or the ferroptosis inhibitor ferrostatin-1 (Fer-1, 1 μM) for 7 days (n
628 = 4, ****$P < 0.0001$). **d**, Representative fluorescence images of human kidney fibroblasts after 4
629 days at 4°C with no treatment, 1 μM Fer-1, 1 μM RSL3, or 1 μM Fer-1 and 1 μM RSL3. Cultures
630 were stained with Hoechst 33342 and propidium iodide (PI) to identify live cells. **e**, Gpx4 activity
631 is essential for cold survival in hibernator cells (Syrian hamster embryonic fibroblasts, Greater
632 horseshoe bat embryonic fibroblasts, and 13-lined ground squirrel embryonic fibroblasts) and
633 non-hibernator cells (SV40-immortalized mouse embryonic fibroblasts, human adult kidney
634 fibroblasts, human adult dermal fibroblasts, rat adult dermal fibroblasts, and mouse adult dermal
635 fibroblasts). Cells were placed at 4°C and left untreated, treated with RSL3 (1 μM), and/or
636 ferrostatin-1 (Fer-1, 1 μM) for 7 days (n = 4). **f**, Expanded Day 4 data from **e)** indicates that
637 Gpx4 activity is essential for fibroblast survival in the cold across several hibernator and non-
638 hibernator species. Cells were placed at 4°C and left untreated or treated with RSL3 (1 μM)
639 and/or ferrostatin-1 (Fer-1, 1 μM) for 7 days (n = 4, ****$P < 0.0001$). **g-h**, Gpx4 activity is
640 essential in **g)** mouse primary cortical neuron cultures and **h)** hamster primary cortical neuron
641 cultures. Cells were placed at 4°C and left untreated, treated with RSL3 (1 μM) and/or the
642 ferroptosis inhibitor ferrostatin-1 (Fer-1, 1 μM) for 1 or 4 days (n = 4). RSL3 treatment increased
643 cell death, which was rescued by ferrostatin-1. All values show mean ± SEM, with significance
644 measured by one-way ANOVA adjusted for multiple comparisons with Tukey's HSD. *$P < 0.05$;
645 **$P < 0.01$; ***$P < 0.001$; ****$P < 0.0001$; ns $P > 0.05$.
646
647
648
649 **Tables**

650 **Table S1. Significant genes from Cycle 3 of genome-wide BHK-21 screen (median log2**
651 **fold-change < -1 or > 1 and FDR < 0.1)**

Gene	Median Log2FC	FDR
Rps29	1.3794	0.017327
Dld	-1.7915	0.003094
Eefsec	-2.1607	0.000707
Gpx4	-2.2215	0.000707
Lias	-1.1881	0.011251
Lipt1	-1.1444	0.05562
Pstk	-2.3621	0.000707
Secisbp2	-1.1041	0.000707
Sepsecs	-2.3116	0.000707
Ybey	-1.5789	0.017492

652
653 **Table S3. Significant genes from 15 days 4°C of genome-wide BHK-21 screen (median**
654 **log2 fold-change < -0.5 or > 0.5 and FDR < 0.1)**

Gene	Median Log2FC	FDR
LOC101827392	0.5431	0.066832
Eefsec	-0.81913	0.00165
Gpx4	-1.5133	0.00165
Secisbp2	-0.74996	0.00165

655
656 **Table S4. Significant genes from Cycle 3, 4°C + ferrostatin-1 vs 4°C of genome-wide K562**
657 **screen (median log2 fold-change < -0.5 or > 0.5 and FDR < 0.1)**

Gene	Median Log2FC	FDR
UBA3	0.59092	0.035754
PSTK	0.85375	0.000707
GPX4	1.3025	0.000707
CMIP	0.83519	0.09946
OXSM	0.82371	0.003094
HSCB	1.0999	0.060891
FTH1	1.4415	0.000707
SEPHS2	0.98322	0.000707
EEFSEC	0.91866	0.000707
FDXR	1.2588	0.000707
SEPSECS	0.9745	0.000707

658
659
660
661
662

663 **Methods**

664 **Cell culture**

665 Two hibernator-derived (BHK-21, HaK) and four non-hibernator-derived (HT1080, RPE1, HeLa,
666 K562) cell lines were used. All cells were purchased from ATCC. K562 cells were cultured in
667 Roswell Park Memorial Institute (RPMI) 1640 Medium (Gibco #11875093) supplemented with
668 10% fetal bovine serum (GeminiBio #100-106) and 1% penicillin/streptomycin. The remaining
669 cells were cultured in Dulbecco's modified Eagle's medium (DMEM) (Thermo Fisher Scientific
670 #12430054) supplemented with 10% fetal bovine serum (GeminiBio #100-106) and 1%
671 penicillin/streptomycin (Thermo Fisher Scientific #15140122).

672

673 **Cell viability assay**

674 Cells were seeded on 24-well culture plates at 50,000 cells per well and allowed to adhere for
675 24 hours at 37°C. Cells were then placed at 4°C with 5% CO_2 for varying time periods (1, 4, or 7
676 days), with a 30-minute rewarming at 37°C before assessing cell viability via trypan blue (TB)
677 (Thermo Fisher Scientific #15250061) staining. To assess cell viability using the TB assay, cells
678 were washed with PBS (Thermo Fisher Scientific #10010023), trypsinized and centrifuged at
679 300 x g for 3 minutes. The resulting pellet was resuspended in media, TB was added to a final
680 concentration of 0.2%, and cells were manually counted using a hemocytometer.

681

682 **Cell death assay (LDH)**

683 The amount of LDH in the supernatant was measured using the LDH-Glo Cytotoxicity Assay
684 (Promega J2380) following the manufacturer's protocol. The samples were mixed with reagents
685 on microplates, and luminescence was measured after a 30-minute incubation at room
686 temperature. The maximum amount of LDH in each was measured by fully lysing replicate wells
687 with 2% Triton X-100 (Thermo Fisher Scientific #A16046.AE). Background LDH signal was
688 measured from media-only wells and subtracted from sample values before normalization to
689 fully lysed wells in order to determine the amount of cytotoxicity per sample.

690

691 **Compound sources**

692 ML162 (SML0521), RSL3 (SML2234), erastin (E7781), 2'2'-Bipyridyl (D216305), and
693 necrostatin-1 (N9037°C) were obtained from MilliporeSigma. Ferrostatin-1 (S7243), Liproxstatin-
694 1 (S7699), and z-VAD-FMK (S7023) were purchased from Selleck Chemicals LLC.
695 Deferoxamine mesylate (ab120727) was purchased from Abcam.

696

697 **Genome-wide library design**

698 sgRNAs targeting the hamster genome build GCF_017639785.1 (BCM_Maur_2.0) were
699 designed based on NCBI Refseq gene annotations. Protein-coding regions of all gene exons
700 were filtered to retain only the most constitutively expressed exons and extended 20 nt on each
701 end. These regions were provided as input for CRISPOR[49] to pick and score all potential
702 guides. For each gene, guides were filtered by potential problem flags and then ranked by an
703 overall score derived from its efficiency (the Doench16/Fusi score), a custom motif penalty, a
704 fractional frameshift (from the Lindel score and the fractional distance to the beginning of the
705 region), and its specificity (derived from the MIT specificity score). For each gene, after the
706 guide with the best score was chosen, subsequent guides were also penalized by a location
707 score, adding a penalty for presence in the same exon and proximity to previously selected
708 guides for the same gene. If more than ten potential guides were identified for a gene, the ten
709 with the highest scores were selected.
710
711 For the human genome-wide library, we obtained a list of protein-coding genes in human based
712 on Ensembl release 98. The top five sgRNAs were picked for protein-coding genes and
713 controls, for a total of 102223 sgRNAs. Human intergenic sgRNAs were chosen by first
714 subsetting the list of all designed intergenic-region-targeted sgRNAs by Rank = 1, then requiring
715 the sgRNAs to target only one genomic locus. This list of 465 sgRNAs was ranked by MIT
716 specificity score in descending order, and the top 449 sgRNAs were chosen.
717

718 **Library cloning**

719 For the hamster library, 214,116 unique protospacer sequences targeting ~21,000 unique gene
720 symbols (> 99% with 10 sgRNAs/gene symbol), along with 2,299 intergenic-targeting and 250
721 nontargeting sequences were synthesized as an oligonucleotide pool (Agilent Technologies).
722 Separately, for the human library, 98,077 unique protospacer sequences targeting ~19,600
723 Ensembl transcript IDs (> 99.9% with 5 sgRNAs/gene), 449 intergenic-targeting sequences, 50
724 non-targeting sequences, and one sequence targeting the *AAVS1* safe harbor locus were
725 synthesized as an oligonucleotide pool (Agilent Technologies). A guanine nucleotide was
726 prepended to each 20-nucleotide protospacer sequence that began with A, C, or T. For both
727 hamster and human libraries, homology arms were prepended (5'-
728 TATCTTGTGGAAAGGACGAAACACC-3') and appended (5'-
729 GTTTAAGAGCTATGCTGGAAACAGCATAGC-3'). Additional adapters were pre- and appended
730 to the hamster library to enable subpool amplification if desired (subpool 1: 5'-
731 TCGGTGTATTGCTAGTGCGAACCCA-3' and 5'-ATCGTGTGAAAGGTGCCGCTATTGC-3';
732 subpool 2: 5'-GGTTCGTTCTACACATGGAAGCGGC-3' and 5'-
733 GAGGACTTCGAGTAGAACGCTGGCG-3'). Oligonucleotide pools were PCR amplified (forward

primer: 5'-TTTCTTGGCTTTATATATCTTGTGGAAAGGACGAAACACC-3'; reverse primer: 5'-ATTTAAACTTGCTATGCTGTTTCCAGCATAGCTCTTAAAC-3') and cloned into pLentiCRISPRv2-Opti (a gift from David Sabatini; Addgene plasmid # 163126; http://n2t.net/addgene:163126; RRID:Addgene_163126). Briefly, 0.25 µL of a 100 nM pool was PCR amplified in 50 µL reactions using Q5 HotStart DNA Polymerase (New England Biolabs) for 10 cycles under the following conditions:

1 cycle	98 °C	2 minutes
10 cycles	98 °C	10 seconds
	55-62 °C	15 seconds
	72 °C	15 seconds
1 cycle	72 °C	2 minutes
1 cycle	4 °C	hold

All concentration steps were performed using a DNA Clean and Concentrator-5 kit (ZymoResearch). Amplification from 8 gradient annealing reactions (55-62 °C) was assessed, and successful reactions were pooled and concentrated. The vector was digested overnight at 37 °C with FastDigest Esp3I and FastAP (ThermoFisher Scientific), gel purified using a Zymoclean gel DNA recovery kit (ZymoResearch), and concentrated. NEBuilder HiFi DNA Assembly Master Mix (New England Biolabs) was used in 2 x 40-80 µL bulk assembly reactions, for a combined total reaction volume of 160 µL containing 4 µg of vector and 160 ng of PCR amplicon (hamster) or 120 µL total containing 3 µg of vector and 120 ng of PCR amplicon (human). Each bulk reaction was distributed in 5 µL aliquots and incubated for 10 minutes at 52.2 °C, pooled, concentrated, introduced into Endura Electrocompetent DUO cells (Lucigen) by electroporation, and plated on 8-16 LB agar with 75 µg/mL carbenicillin in 245 mm x 245 mm square bioassay dishes. A dilution series was also plated to assess electroporation efficiency. Cells were incubated overnight at 30 °C, collected, and DNA was isolated using a ZymoPURE II Plasmid DNA Maxiprep kit (ZymoResearch). Plasmid from separate electroporations was combined proportionally based on electroporation efficiency for a combined total library coverage of > 50-fold for each library. Sequence representation in the libraries was assessed as described below.

Lentivirus production for CRISPR-Cas9 screen

767 For large-scale virus production, HEK-293T ($1.5x10^7$) cells were seeded in T175 cm^2 flasks in
768 DMEM (Thermo Fisher Scientific #12430054) supplemented with 10% fetal bovine serum
769 (GeminiBio #100-106). Media was changed 24 hours later to 20 mL viral production medium:
770 IMDM (Thermo Fisher Scientific #1244053) supplemented with 20% heat-inactivated fetal
771 bovine serum (GeminiBio #100-106). Cells were transfected 8 hours later with a mix containing
772 76.8 µL Xtremegene-9 transfection reagent (MilliporeSigma #06365779001), 3.62 µg pCMV-
773 VSV-G (Addgene plasmid # 8454; http://n2t.net/addgene:8454; RRID:Addgene_8454)[50], 8.28
774 µg psPAX2 (a gift from Didier Trono; Addgene plasmid # 12260; http://n2t.net/addgene:12260;
775 RRID:Addgene_12260), and 20 µg sgRNA/Cas9 plasmid and Opti-MEM (Thermo Fisher
776 Scientific #11058021) to a final volume of 1 mL. Media was changed 16 hours later to 55 mL
777 fresh viral production medium. Viral supernatant was collected and filtered through a 0.45 µm
778 filter and aliquoted 48 hours post-transfection, then stored at -80°C until use.
779
780 **CRISPR screen in K562 cells**
781 K562 cells ($3.9x10^8$) were transduced with a pooled genome-wide lentiviral sgRNA library in a
782 Cas9-containing vector at MOI <1. The transduced cells were selected with 3 µg/mL puromycin
783 (Thermo Fisher Scientific #A1113803), and $1x10^8$ cells were passaged every 48-72 hours at a
784 density of $6x10^5$ cells/T175 cm^2 flask in 45 mL RPMI 1640 (Gibco #11875093) medium
785 supplemented with 10% fetal bovine serum (GeminiBio #100-106) and 1%
786 penicillin/streptomycin for the duration of the screen. At 5 days post-puromycin selection, $1x10^8$
787 cells were exposed to the cold with or without 1 µM ferrostatin-1 (Selleck Chemicals #S7243).
788 K562 cells ($1x10^8$) were collected from the each of surviving populations after cold exposure
789 and/or rewarming as well as a matched untreated population. Genomic DNA was isolated using
790 the QIAmp DNA Blood Maxiprep kit (Qiagen # 51192), and high-throughput sequencing libraries
791 were prepared.
792
793 **CRISPR screen in BHK-21 cells**
794 BHK-21 cells ($8.55x10^8$) were transduced with a pooled genome-wide lentiviral sgRNA library in
795 a Cas9-containing vector at an MOI of 0.25. Transduced cells were selected with 2 µg/mL
796 puromycin (Thermo Fisher Scientific #A1113803), and $2.56x10^8$ cells were passaged every 48-
797 72 hours at a density of $5x10^6$ cells/15-cm dish in DMEM (Thermo Fisher Scientific #12430054)
798 medium supplemented with 10% fetal bovine serum (GeminiBio #100-106) and 1%
799 penicillin/streptomycin for the duration of the screen. At 6 days post-puromycin selection,
800 $2.56x10^8$ cells were exposed to the cold. Cells ($2.4x10^8$) were collected from each of the

801 surviving populations after cold exposure and/or rewarming as well as from a matched
802 untreated population. During the cycles, cells were placed at 4°C for 4 days, then rewarmed to
803 37°C for 24 hours, reseeded, and after a further 24 hours at 37°C were placed back at 4°C to
804 begin a subsequent cycle. Genomic DNA was isolated using the QIAmp DNA Blood Maxiprep
805 kit (Qiagen # 51192), and high-throughput sequencing libraries were prepared.
806
807 **Sequencing library preparation**
808 The QIAamp DNA Blood Maxiprep Kit (Qiagen # 51192) was used to extract genomic DNA
809 (gDNA) from cell pellets of 2.5-5x10^7 cells according to manufacturer's instructions with minor
810 modifications: QIAGEN Protease was replaced with 500 µL of 10 mg/mL Proteinase K
811 (MilliporeSigma # 3115879001) in water, and cells were lysed overnight; centrifugation was
812 performed for 2 minutes and 5 minutes after the first and second wash, respectively; 1 mL of
813 water preheated to 70 °C was used to elute gDNA, followed by centrifugation for 5 minutes.
814 gDNA was quantified using the Qubit dsDNA HS Assay kit (Thermo Fisher Scientific #Q32851).
815 PCR amplification of sgRNA sequences was performed in 50 µL reactions using ExTaq
816 Polymerase (Takara Bio #RR001B) with the following program:
817
818 1 cycle 95 °C 5 minutes
819 16, 24, or 28 cycles 95 °C 10 seconds
820 60 °C 15 seconds
821 72 °C 45 seconds
822 1 cycle 72 °C 5 minutes
823 1 cycle 4 °C hold
824
825 Using the following primers:
826 Forward: 5'- AATGATACGGCGACCACCGAGATCTACACCCCACTGACGGGCACCGGA - 3'
827 Reverse: 5'- CAAGCAGAAGACGGCATACGAGATCnnnnnnTTTCTTGGGTAGTTTGCAGTTTT
828 - 3'
829 Where "nnnnnn" denotes the barcode used for demultiplexing.
830
831 Plasmid libraries were amplified for 16 cycles using 10 ng input per 50 µL reaction. gDNA was
832 initially amplified for 24 (human) or 28 (hamster) cycles in 50 µL test PCR reactions with 1, 3, 4,
833 5, or 6 µg input. An additional 20-75 reactions were performed using 3-6 µg per reaction
834 (sampling 150 µg or 300 µg gDNA total for human and hamster screens, respectively). Select-a-

835 Size DNA Clean and Concentrator (Zymo Research #D4080) or HighPrep PCR (MagBio
836 Genomics) was used to purify 95-100 µL of each pooled sample, which were eluted with 12-20
837 µL water and quantified using the Qubit dsDNA HS Assay kit prior to sequencing for 50 cycles
838 on an Illumina Hiseq 2500 or NovaSeq using the following primers:
839
840 Read 1 sequencing primer: 5'-
841 GTTGATAACGGACTAGCCTTATTTAAACTTGCTATGCTGTTTCCAGCATAGCTCTTAAAC - 3'
842 Index sequencing primer: 5'-
843 TTTCAAGTTACGGTAAGCATATGATAGTCCATTTTAAAACATAATTTTAAAACTGCAAACTAC
844 CCAAGAAA - 3'
845
846 **CRISPR screen data analysis**
847 Sequencing reads from the human screen were trimmed and mapped to the sgRNA library
848 using Bowtie version 1.0.0[51], allowing no mismatches, and counted. Sequencing reads from the
849 hamster screen were trimmed and mapped to the sgRNA library using a combination of
850 command line prompts and a custom Python function which generated a dataframe of counts
851 which perfectly (no permissibility for any base mismatches) matched sequenced reads to the full
852 guide library (code supplied on Github). Data from both human and hamster screens was
853 similarly analyzed using MAGeCK version 0.5.9.5[52] using a gene test false discovery rate (FDR)
854 threshold of 0.05, the FDR method for p-value adjustment, and the median as the gene-level
855 scoring metric.
856
857 PANTHER overrepresentation test was conducted on a set of 204 genes (FDR < 0.1) from the
858 third cycle of the human K562 CRISPR-Cas9 screen ['Analyzed List']. A list of genes expressed
859 in K562 cells at 37°C collected from bulk RNA sequencing was used as the ['Reference List']:
860 https://pantherdb.org/tools/compareToRefList.jsp. Fisher's Exact test type and false discovery
861 rate correction were utilized. Bulk RNA sequencing of K562 cells at 37°C was conducted by
862 generating a cDNA library prepared by depleting rRNA using the NEBNext rRNA Depletion Kit
863 (Human/Mouse/Rat) (New England Biolabs) and then the NEBNext Ultra II Directional RNA
864 Library Prep Kit (New England Biolabs). cDNA libraries were amplified using appropriate
865 multiplexed index primers for PCR.
866
867 Data was visualized using R version 4.2.1[53] corrplot package version 0.92[54] and base graphics,
868 and GraphPad Prism version 10.

869

870 **Generation of stable CRISPR/Cas9-targeted cell lines**

871 Homology arms were prepended (5'-TATCTTGTGGAAAGGACGAAACACC-3') and appended
872 (5'-GTTTAAGAGCTATGCTGGAAACAGCATAGC-3') to the top two ranked human or hamster
873 *GPX4*-targeting guides from the genome-wide screens. These guides were PCR amplified and
874 cloned into pLentiCRISPRv2-Opti (a gift from David Sabatini; Addgene plasmid # 163126;
875 http://n2t.net/addgene:163126; RRID:Addgene_163126). K562 and BHK-21 cells were then
876 infected with LentiCRISPRv2. Transduced cells were selected with 3 µg/mL puromycin (Thermo
877 Fisher Scientific #A1113803) for K562 cells and 2 µg/mL for BHK-21 cells beginning two days
878 after infection. After one passage, cells were sorted (BD FACSAria™ Fusion Flow Cytometer)
879 into 96-well plates, at one cell per well to generate clonal knockout cell lines. Cells were cultured
880 in media with 2.5 µM liproxstatin-1 (Selleck Chemicals #S7699) to prevent cell death. Western
881 blotting was used to confirm GPX4 loss in individual knockout clones prior to further use.

882

883 Human sgRNA:
884 5'- CGTGTGCATCGTCACCAACG - 3'
885 5'- CTTGGCGGAAAACTCGTGCA - 3'

886

887 Hamster sgRNA:
888 5'- CGTGTGCATCGTCACCAACG - 3'
889 5'- CTTGGCTGAGAATTCGTGCA - 3'

890

891 **Generation of CRISPR/Cas9-targeted human kidney fibroblast pooled cells**

892 Primary human kidney fibroblasts were infected with LentiCRISPRv2 with sgRNAs targeting
893 *GPX4*, using the top two ranked *GPX4*-targeting guides from the genome-wide human k562
894 screen. Transduced cells were selected with 1 µg/mL puromycin (Thermo Fisher Scientific
895 #A1113803) beginning four days after infection. Cells were cultured in media with 2.5 µM
896 liproxstatin-1 (Selleck Chemicals #S7699) to prevent cell death. Western blotting was used to
897 confirm GPX4 loss in individual knockout clones prior to further use.

898

899 **Immuoblotting**

900 Cells were plated at $6x10^5$ cells per well in a 6-well plate and maintained overnight at 37°C.
901 Cells were then collected when wells were confluent. The media was aspirated, and cells were
902 washed with ice-cold PBS (Thermo Fisher Scientific #10010023). Cells were scraped in 100 µL

903 of RIPA buffer (150 mM NaCl, 1% Triton X-100, 0.5% Na-Dexycholate, 0.1% SDS, 50 mM Tris,
904 pH 8) with protease inhibitors (MilliporeSigma #04693159001) and collected in microcentrifuge
905 tubes. The contents were then vortexed for 30 minutes at 4°C and centrifuged at 16000 x g for
906 20 minutes at 4°C. Protein content of the samples was measured using the Pierce BCA Protein
907 Assay kit (Thermo Fisher Scientific #23225) and resuspended in 100 µL of RIPA buffer with
908 protein loading dye (10% SDS, 500 mM DTT, 50% Glycerol, 250 mM Tris-HCl and 0.5%
909 bromophenol blue dye, pH 6.8). Protein samples were boiled for 5 minutes at 95°C, vortexed,
910 and centrifuged at 16000 x g for 5 minutes before loading onto a gel. The gel was run at 120 V
911 for 2 hours before being transferred to a Polyvinylidene difluoride (PVDF) membrane (Thermo
912 Fisher Scientific #88518). The transfer cassette was run at 45 V for 2 hours. The membranes
913 were then transferred to 5% milk TBST (1X Tris-Buffered Saline, 0.1% Tween® 20 Detergent)
914 and shaken for 15 minutes before being washed in TBST. Primary antibodies recognizing GPX4
915 (Abcam #ab41787) or HA (Cell Signaling Technology #3724) were added at 1:1000 in 5% BSA
916 (MilliporeSigma #A9418) and incubated overnight at 4°C. The membrane was then washed 3
917 times in 1x TBST and 1:3000 anti-rabbit secondary antibody (Cell Signaling Technology #7074)
918 in 5% milk TBST was added. Membranes were incubated for 1 hour at room temperature and
919 washed 3x in 1x TBST. Membranes were then incubated in Pierce™ ECL Western Blotting
920 Substrate (Thermo Fisher Scientific #32106) for 5 minutes before imaging.
921
922 **Generation of HA-GPX4 and HA-GFP overexpression constructs**
923 To generate GPX4-overexpression lines, entire human *GPX4* (cytosolic; NM_001367832.1) and
924 hamster *Gpx4* were amplified from the cDNA of K562 and BHK-21 cells, respectively. The
925 cloned transcript fragments include the 3' UTR that contains the SECIS element necessary for
926 selenocysteine incorporation. The *GPX4* genomic DNA fragments were cloned into pLJM1
927 (Addgene plasmid # 19319; http://n2t.net/addgene:19319; RRID:Addgene_19319) and
928 confirmed via sequencing. To create GPX4 mutants, (U46S), non-overlapping primers were
929 used to create mutations via inverse PCR, as previously described[55], converting the UGA stop
930 codon to UCA, encoding serine. GFP was amplified from pLJM1-EGFP (Addgene plasmid #
931 19319; http://n2t.net/addgene:19319; RRID:Addgene 19319) with Gibson overhangs to enable
932 insertion into a lentivirus vector. HA-GPX4 and HA-GFP DNA fragments were then amplified by
933 PCR and cloned into blasticidin lentiviral vectors [gift from Whitney Henry at the Whitehead
934 Institute for Biomedical Research] using standard cloning methods, with point mutations in the
935 PAM and guide sequences to prevent targeting of exogenously expressed *GPX4*.
936

937 HEK-293T cells ($5x10^5$) were seeded in 2 wells of a 6-well plate in DMEM (Thermo Fisher
938 Scientific #12430054) supplemented with 10% fetal bovine serum (GeminiBio #100-106).
939 Media was changed 16 hours later to 2 mL per well of viral production medium: IMDM (Thermo
940 Fisher Scientific #1244053) supplemented with 20% heat-inactivated fetal bovine serum
941 (GeminiBio #100-106). Cells were transfected 8 hours later with a mix containing 4.22 µL
942 Xtremegene-9 transfection reagent (MilliporeSigma #06365779001), 181 ng pCMV-VSV-G
943 (Addgene plasmid # 8454; http://n2t.net/addgene:8454; RRID:Addgene_8454)[50], 414 ng
944 psPAX2 (a gift from Didier Trono; Addgene plasmid # 12260; http://n2t.net/addgene:12260;
945 RRID:Addgene_12260), and 1 µg HA-GPX4 or HA-GFP plasmid and Opti-MEM (Thermo Fisher
946 Scientific #11058021) to a final volume of 50 µL per well. Media was changed 16 hours later to
947 2.5 mL per well of fresh viral production medium. Viral supernatant was collected and aliquoted
948 48 hours post-transfection, then stored at -80°C until use.
949
950 K562 or BHK-21 cells ($6x10^5$, wild-type and GPX4 knockout clones) were transduced with the
951 lentiviral HA-tagged GPX4 or GFP in the presence of 10 µg/mL polybrene. After 8 hours of
952 incubation at 37°C, media was changed to virus-free media. After 48 hours, the transduced cells
953 were selected with blasticidin (Thermo Fisher Scientific #A1113903) at a concentration of 6
954 µg/mL for K562 cells and 4 µg/mL for BHK-21 cells. Overexpression of GPX4 and GFP was
955 confirmed via immunoblotting.
956
957 **Primary cell culture**
958 Three hibernator (13-lined ground squirrel postnatal dermal fibroblasts [gift from Wei Li at Duke
959 University], SV40-immortalized Greater horseshoe bat embryonic dermal fibroblasts [gift from
960 Rudolf Jaenisch at the Whitehead Institute for Biomedical Research], and Syrian golden
961 hamster embryonic primary dermal fibroblasts [isolated]) and five non-hibernator (mouse
962 embryonic SV40-immortalized dermal fibroblasts [gift from Jonathan Weissman at the
963 Whitehead Institute for Biomedical Research], adult human kidney fibroblasts [purchased from
964 ATCC], adult human dermal fibroblasts [purchased from ATCC], adult rat dermal fibroblasts
965 [purchased from ATCC], and adult mouse fibroblasts [purchased from ATCC]) primary cells
966 were cultured in Dulbecco's modified Eagle's medium (Thermo Fisher Scientific #12430054)
967 supplemented with 10% fetal bovine serum (GeminiBio #100-106) and 1%
968 penicillin/streptomycin (Thermo Fisher Scientific #15140122). Cells were seeded on 24-well
969 culture plates at ~50,000 cells per well and allowed to adhere for 24 hours at 37°C. Cells were
970 then placed at 4°C with 5% CO_2 for varying time periods (1, 4, or 7 days), with a 30-minute

971 rewarming at 37°C before assessing cell viability via trypan blue (TB) (Thermo Fisher Scientific
972 #15250061) staining. To assess cell viability using the TB assay, cells were washed with PBS
973 (Thermo Fisher Scientific #10010023), trypsinized and centrifuged at 300 x g for 3 minutes. The
974 resulting pellet was resuspended in media, TB was added to a final concentration of 0.2%, and
975 cells were manually counted using a hemocytometer.
976
977 **Primary neuron isolation and culture**
978 Primary Syrian golden hamster and C57BL/6 mouse cortical neurons were isolated at postnatal
979 day 0. The day before isolation, standard tissue culture treated plates were coated with 3 µg/mL
980 Poly-L-Ornithine (MilliporeSigma #P4957) and warmed at 37°C for 24 hours. The morning of
981 isolation, wells were washed with 1X PBS (Thermo Fisher Scientific #10010023). To isolate
982 neurons, pups were placed on ice for 2-5 minutes until movement ceased. Afterwards, they
983 were washed with 10% ethanol, decapitated, and their heads placed in a 10x dissociation media
984 bath (10.16 g $MgCl_2$ hexahydrate and 11.915 g HEPES in 450 mL HBSS brought to a pH of 7
985 using NaOH with subsequent addition of 1.182 g of kynurenic acid heated to 65% while stirring
986 until the solution was fully dissolved and cooled to room temperature and adjusted to a pH of
987 7.2. The dissociation media was then diluted from 10X to 1X in HBSS and filtered through a
988 0.22-µm vacuum filter). Dissected brains were placed in fresh dissociation media, where the
989 cortices were dissected out and transferred to 50 mL Falcon tubes on ice containing 1X
990 dissociation media. Afterwards, the dissociation media was removed from the cortices and
991 replaced with papain solution (5 mL 1x dissociation media, 5-7 grains of L-Cyteine, and 172 µL
992 Worthington papain [crystalline suspension in 50mM sodium acetate, pH 4.5 incubated in
993 1.1mM EDTA, 0.067mM mercaptoethanol and 5.5mM cysteine-HCl at 37°C. Activates to 20
994 units per 1 mg protein]) that was preheated to 37°C for 30 minutes. The cortices were incubated
995 in the papain solution for 3-5 minutes at 37°C. Afterwards, the papain solution was replaced with
996 trypsin inhibitor solution (10 mg of trypsin inhibitor dissolved in 10 mL of 1X dissociation media,
997 preheated to 37°C) and incubated subsequently at 37°C for 3-5 minutes, repeated 3 times.
998 Afterwards, the trypsin inhibitor solution was carefully removed and replaced with 6 mL of
999 preheated complete neurobasal media (5 mL of GlutaMAX5, 10 mL of B-27, 5 mL of
1000 penicillin/streptomycin in neurobasal media filtered through a 0.22-µm vacuum filter). Using a 5
1001 mL pipette tip, corticies were triturated until no tissue clumps were present. The cortices were
1002 then passed through a 100-µm cell strainer to remove large debris and centrifuged at 300 x g for
1003 3 minutes before resuspension in 5 mL of complete neurobasal media before plating at a

density of 50,000 mixed cortical neuron isolated cells per well of a 24 well plate. Subsequently, 50% of the media was replaced every second day with fresh 37°Ç pre-warmed media.

Statistical analyses and software information

Data are generally plotted as mean ± S.E.M. unless otherwise indicated. No statistical methods were used to predetermine sample sizes. Unless otherwise indicated, all replication numbers in the figure legends (n) indicate biological replicates. Statistical significance was determined using a two-tailed Student's T-test, one-way ANOVA, or two-way ANOVA using Prism 10 software (GraphPad Software) unless otherwise indicated. Statistical significance was set at $p<=0.05$ unless otherwise indicated. Figures were finalized in Adobe Illustrator 2024.

Supplemental information

Document S1. Figures S1-S11

Table S2. Excel file containing hamster screen data, related to Figure 2

Table S5. Excel file containing human screen data, related to Figure 4

Table S6. Excel file containing GO_Biological Processes, related to Figure S8

References

1. Cheshire, W.P. (2016). Thermoregulatory disorders and illness related to heat and cold stress. Autonomic Neuroscience *196*, 91–104. https://doi.org/10.1016/j.autneu.2016.01.001.

2. Physiology, Thermal Regulation - StatPearls - NCBI Bookshelf https://www.ncbi.nlm.nih.gov/books/NBK499843/.

3. Tan, C.L., and Knight, Z.A. (2018). Regulation of body temperature by the nervous system. Neuron *98*, 31–48. https://doi.org/10.1016/j.neuron.2018.02.022.

4. Morrison, S.F., and Nakamura, K. (2019). Central Mechanisms for Thermoregulation. Annu Rev Physiol *81*, 285–308. https://doi.org/10.1146/annurev-physiol-020518-114546.

5. Hendriks, K.D.W., Joschko, C.P., Hoogstra-Berends, F., Heegsma, J., Faber, K.-N., and Henning, R.H. (2020). Hibernator-Derived Cells Show Superior Protection and Survival in Hypothermia Compared to Non-Hibernator Cells. IJMS *21*, 1864. https://doi.org/10.3390/ijms21051864.

6. Ou, J., Ball, J.M., Luan, Y., Zhao, T., Miyagishima, K.J., Xu, Y., Zhou, H., Chen, J., Merriman, D.K., Xie, Z., et al. (2018). iPSCs from a Hibernator Provide a Platform for Studying Cold Adaptation and Its Potential Medical Applications. Cell *173*, 851-863.e16. https://doi.org/10.1016/j.cell.2018.03.010.

1038 7. Hendriks, K.D.W., Lupi, E., Hardenberg, M.C., Hoogstra-Berends, F., Deelman, L.E., and
1039 Henning, R.H. (2017). Differences in mitochondrial function and morphology during cooling
1040 and rewarming between hibernator and non-hibernator derived kidney epithelial cells.

1041 8. Anegawa, D., Sugiura, Y., Matsuoka, Y., Sone, M., Shichiri, M., Otsuka, R., Ishida, N.,
1042 Yamada, K., Suematsu, M., Miura, M., et al. (2021). Hepatic resistance to cold ferroptosis in
1043 a mammalian hibernator Syrian hamster depends on effective storage of diet-derived α-
1044 tocopherol. Commun Biol *4*, 796. https://doi.org/10.1038/s42003-021-02297-6.

1045 9. Park, H.G., Han, S.I., Oh, S.Y., and Kang, H.S. (2005). Cellular responses to mild heat
1046 stress. CMLS, Cell. Mol. Life Sci. *62*, 10–23. https://doi.org/10.1007/s00018-004-4208-7.

1047 10. Richter, K., Haslbeck, M., and Buchner, J. (2010). The Heat Shock Response: Life on the
1048 Verge of Death. Molecular Cell *40*, 253–266. https://doi.org/10.1016/j.molcel.2010.10.006.

1049 11. Karunanithi, S., and Brown, I.R. (2015). Heat shock response and homeostatic plasticity.
1050 Front. Cell. Neurosci. *9*. https://doi.org/10.3389/fncel.2015.00068.

1051 12. Kruuv, J., Glofcheski, D., Cheng, K.H., Campbell, S.D., Al-Qysi, H.M., Nolan, W.T., and
1052 Lepock, J.R. (1983). Factors influencing survival and growth of mammalian cells exposed to
1053 hypothermia. I. Effects of temperature and membrane lipid perturbers. J Cell Physiol *115*,
1054 179–185. https://doi.org/10.1002/jcp.1041150212.

1055 13. Hochachka, P.W. (1986). Defense strategies against hypoxia and hypothermia. Science
1056 *231*, 234–241. https://doi.org/10.1126/science.2417316.

1057 14. Rule, G.S., Frim, J., Thompson, J.E., Lepock, J.R., and Kruuv, J. (1978). The effect of
1058 membrane lipid perturbers on survival of mammalian cells to cold. Cryobiology *15*, 408–414.
1059 https://doi.org/10.1016/0011-2240(78)90059-7.

1060 15. Zachariassen, K.E. (1991). Hypothermia and cellular physiology. Arctic Med Res *50 Suppl*
1061 *6*, 13–17.

1062 16. Heller, H.C., and Hammel, H.T. (1972). CNS control of body temperature during hibernation.
1063 Comp Biochem Physiol A Comp Physiol *41*, 349–359. https://doi.org/10.1016/0300-
1064 9629(72)90066-7.

1065 17. Sunagawa, G.A., and Takahashi, M. (2016). Hypometabolism during Daily Torpor in Mice is
1066 Dominated by Reduction in the Sensitivity of the Thermoregulatory System. Sci Rep *6*,
1067 37011. https://doi.org/10.1038/srep37011.

1068 18. Geiser, F. (2004). Metabolic rate and body temperature reduction during hibernation and
1069 daily torpor. Annu Rev Physiol *66*, 239–274.
1070 https://doi.org/10.1146/annurev.physiol.66.032102.115105.

1071 19. Chayama, Y., Ando, L., Tamura, Y., Miura, M., and Yamaguchi, Y. (2016). Decreases in
1072 body temperature and body mass constitute pre-hibernation remodelling in the Syrian
1073 golden hamster, a facultative mammalian hibernator. R Soc Open Sci *3*, 160002.
1074 https://doi.org/10.1098/rsos.160002.

1075 20. Park, K.J., Jones, G., and Ransome, R.D. (2000). Torpor, arousal and activity of hibernating
1076 Greater Horseshoe Bats (Rhinolophus ferrumequinum). Functional Ecology *14*, 580–588.
1077 https://doi.org/10.1046/j.1365-2435.2000.t01-1-00460.x.

1078 21. Cooper, S.T., Richters, K.E., Melin, T.E., Liu, Z., Hordyk, P.J., Benrud, R.R., Geiser, L.R.,
1079 Cash, S.E., Simon Shelley, C., Howard, D.R., et al. (2012). The hibernating 13-lined ground
1080 squirrel as a model organism for potential cold storage of platelets. Am J Physiol Regul
1081 Integr Comp Physiol *302*, R1202–R1208. https://doi.org/10.1152/ajpregu.00018.2012.

1082 22. Heldmaier, G., Ortmann, S., and Elvert, R. (2004). Natural hypometabolism during
1083 hibernation and daily torpor in mammals. Respiratory Physiology & Neurobiology *141*, 317–
1084 329. https://doi.org/10.1016/j.resp.2004.03.014.

1085 23. Harris, R.A., Raveendran, M., Lyfoung, D.T., Sedlazeck, F.J., Mahmoud, M., Prall, T.M.,
1086 Karl, J.A., Doddapaneni, H., Meng, Q., Han, Y., et al. (2022). Construction of a new
1087 chromosome-scale, long-read reference genome assembly for the Syrian hamster,
1088 Mesocricetus auratus. Gigascience *11*, giac039.
1089 https://doi.org/10.1093/gigascience/giac039.

1090 24. Hart, T., Tong, A.H.Y., Chan, K., Van Leeuwen, J., Seetharaman, A., Aregger, M.,
1091 Chandrashekhar, M., Hustedt, N., Seth, S., Noonan, A., et al. (2017). Evaluation and Design
1092 of Genome-Wide CRISPR/SpCas9 Knockout Screens. G3 (Bethesda) *7*, 2719–2727.
1093 https://doi.org/10.1534/g3.117.041277.

1094 25. Mirabello, L., Macari, E.R., Jessop, L., Ellis, S.R., Myers, T., Giri, N., Taylor, A.M., McGrath,
1095 K.E., Humphries, J.M., Ballew, B.J., et al. (2014). Whole-exome sequencing and functional
1096 studies identify RPS29 as a novel gene mutated in multicase Diamond-Blackfan anemia
1097 families. Blood *124*, 24–32. https://doi.org/10.1182/blood-2013-11-540278.

1098 26. Summer, S., Smirnova, A., Gabriele, A., Toth, U., Fasemore, A.M., Förstner, K.U., Kuhn, L.,
1099 Chicher, J., Hammann, P., Mitulović, G., et al. (2020). YBEY is an essential biogenesis
1100 factor for mitochondrial ribosomes. Nucleic Acids Res *48*, 9762–9786.
1101 https://doi.org/10.1093/nar/gkaa148.

1102 27. Ni, M., Solmonson, A., Pan, C., Yang, C., Li, D., Notzon, A., Cai, L., Guevara, G., Zacharias,
1103 L.G., Faubert, B., et al. (2019). Functional Assessment of Lipoyltransferase-1 Deficiency in
1104 Cells, Mice, and Humans. Cell Rep *27*, 1376-1386.e6.
1105 https://doi.org/10.1016/j.celrep.2019.04.005.

1106 28. Xu, G., Li, W., Zhao, Y., Fan, T., Gao, Q., Wang, Y., Zhang, F., Gao, M., An, Z., and Yang,
1107 Z. (2024). Overexpression of Lias Gene Alleviates Cadmium-Induced Kidney Injury in Mice
1108 Involving Multiple Effects: Metabolism, Oxidative Stress, and Inflammation. Biol Trace Elem
1109 Res *202*, 2797–2811. https://doi.org/10.1007/s12011-023-03883-x.

1110 29. Douce, R., Bourguignon, J., Neuburger, M., and Rébeillé, F. (2001). The glycine
1111 decarboxylase system: a fascinating complex. Trends Plant Sci *6*, 167–176.
1112 https://doi.org/10.1016/s1360-1385(01)01892-1.

1113 30. Weaver, K., and Skouta, R. (2022). The Selenoprotein Glutathione Peroxidase 4: From
1114 Molecular Mechanisms to Novel Therapeutic Opportunities. Biomedicines *10*, 891.
1115 https://doi.org/10.3390/biomedicines10040891.

1116 31. Seibt, T.M., Proneth, B., and Conrad, M. (2019). Role of GPX4 in ferroptosis and its
1117 pharmacological implication. Free Radical Biology and Medicine *133*, 144–152.
1118 https://doi.org/10.1016/j.freeradbiomed.2018.09.014.

1119 32. Varlamova, E.G., Goltyaev, M.V., Novoselov, S.V., Novoselov, V.I., and Fesenko, E.E.
1120 (2013). Selenocysteine biosynthesis and mechanism of incorporation into growing proteins.
1121 Mol Biol *47*, 488–495. https://doi.org/10.1134/S0026893313040134.

1122 33. French, R., and Simonovic, M. (2012). Synthesis and decoding of selenocysteine and
1123 human health. Croatian medical journal *53*, 535–550.
1124 https://doi.org/10.3325/cmj.2012.53.535.

1125 34. Chen, T., Leng, J., Tan, J., Zhao, Y., Xie, S., Zhao, S., Yan, X., Zhu, L., Luo, J., Kong, L., et
1126 al. (2023). Discovery of Novel Potent Covalent Glutathione Peroxidase 4 Inhibitors as Highly
1127 Selective Ferroptosis Inducers for the Treatment of Triple-Negative Breast Cancer. J. Med.
1128 Chem. *66*, 10036–10059. https://doi.org/10.1021/acs.jmedchem.3c00967.

1129 35. Shintoku, R., Takigawa, Y., Yamada, K., Kubota, C., Yoshimoto, Y., Takeuchi, T., Koshiishi,
1130 I., and Torii, S. (2017). Lipoxygenase-mediated generation of lipid peroxides enhances
1131 ferroptosis induced by erastin and RSL3. Cancer Science *108*, 2187–2194.
1132 https://doi.org/10.1111/cas.13380.

1133 36. Sui, X., Zhang, R., Liu, S., Duan, T., Zhai, L., Zhang, M., Han, X., Xiang, Y., Huang, X., Lin,
1134 H., et al. (2018). RSL3 Drives Ferroptosis Through GPX4 Inactivation and ROS Production
1135 in Colorectal Cancer. Front. Pharmacol. *9*. https://doi.org/10.3389/fphar.2018.01371.

1136 37. Hattori, K., Ishikawa, H., Sakauchi, C., Takayanagi, S., Naguro, I., and Ichijo, H. (2017).
1137 Cold stress-induced ferroptosis involves the ASK1-p38 pathway. EMBO Rep *18*, 2067–
1138 2078. https://doi.org/10.15252/embr.201744228.

1139 38. Doll, S., Freitas, F.P., Shah, R., Aldrovandi, M., Da Silva, M.C., Ingold, I., Goya Grocin, A.,
1140 Xavier Da Silva, T.N., Panzilius, E., Scheel, C.H., et al. (2019). FSP1 is a glutathione-
1141 independent ferroptosis suppressor. Nature *575*, 693–698. https://doi.org/10.1038/s41586-
1142 019-1707-0.

1143 39. Bersuker, K., Hendricks, J.M., Li, Z., Magtanong, L., Ford, B., Tang, P.H., Roberts, M.A.,
1144 Tong, B., Maimone, T.J., Zoncu, R., et al. (2019). The CoQ oxidoreductase FSP1 acts
1145 parallel to GPX4 to inhibit ferroptosis. Nature *575*, 688–692. https://doi.org/10.1038/s41586-
1146 019-1705-2.

1147 40. Hu, Q., Wei, W., Wu, D., Huang, F., Li, M., Li, W., Yin, J., Peng, Y., Lu, Y., Zhao, Q., et al.
1148 (2022). Blockade of GCH1/BH4 Axis Activates Ferritinophagy to Mitigate the Resistance of
1149 Colorectal Cancer to Erastin-Induced Ferroptosis. Front Cell Dev Biol *10*, 810327.
1150 https://doi.org/10.3389/fcell.2022.810327.

1151 41. Ma, T., Du, J., Zhang, Y., Wang, Y., Wang, B., and Zhang, T. (2022). GPX4-independent
1152 ferroptosis—a new strategy in disease's therapy. Cell Death Discov. *8*, 1–8.
1153 https://doi.org/10.1038/s41420-022-01212-0.

1154 42. Zhang, W., Dai, J., Hou, G., Liu, H., Zheng, S., Wang, X., Lin, Q., Zhang, Y., Lu, M., Gong,
1155 Y., et al. (2023). SMURF2 predisposes cancer cell toward ferroptosis in GPX4-independent

1156 manners by promoting GSTP1 degradation. Molecular Cell *83*, 4352-4369.e8.
1157 https://doi.org/10.1016/j.molcel.2023.10.042.

1158 43. Sone, M., Mitsuhashi, N., Sugiura, Y., Matsuoka, Y., Maeda, R., Yamauchi, A., Okahashi,
1159 R., Yamashita, J., Sone, K., Enju, S., et al. (2023). Identification of genes supporting cold
1160 resistance of mammalian cells: lessons from a hibernator. Preprint at bioRxiv,
1161 https://doi.org/10.1101/2023.12.27.573489 https://doi.org/10.1101/2023.12.27.573489.

1162 44. Davey, H.M., and Hexley, P. (2011). Red but not dead? Membranes of stressed
1163 Saccharomyces cerevisiae are permeable to propidium iodide. Environ Microbiol *13*, 163–
1164 171. https://doi.org/10.1111/j.1462-2920.2010.02317.x.

1165 45. Kirchhoff, C., and Cypionka, H. (2017). Propidium ion enters viable cells with high
1166 membrane potential during live-dead staining. Journal of Microbiological Methods *142*, 79–
1167 82. https://doi.org/10.1016/j.mimet.2017.09.011.

1168 46. Li, F.-J., Long, H.-Z., Zhou, Z.-W., Luo, H.-Y., Xu, S.-G., and Gao, L.-C. (2022). System Xc -
1169 /GSH/GPX4 axis: An important antioxidant system for the ferroptosis in drug-resistant solid
1170 tumor therapy. Front Pharmacol *13*, 910292. https://doi.org/10.3389/fphar.2022.910292.

1171 47. Forman, H.J., Zhang, H., and Rinna, A. (2009). Glutathione: Overview of its protective roles,
1172 measurement, and biosynthesis. Mol Aspects Med *30*, 1–12.
1173 https://doi.org/10.1016/j.mam.2008.08.006.

1174 48. Yoo, S.-E., Chen, L., Na, R., Liu, Y., Rios, C., Remmen, H.V., Richardson, A., and Ran, Q.
1175 (2012). Gpx4 ablation in adult mice results in a lethal phenotype accompanied by neuronal
1176 loss in brain. Free Radic Biol Med *52*, 1820–1827.
1177 https://doi.org/10.1016/j.freeradbiomed.2012.02.043.

1178 49. Concordet, J.-P., and Haeussler, M. (2018). CRISPOR: intuitive guide selection for
1179 CRISPR/Cas9 genome editing experiments and screens. Nucleic Acids Res *46*, W242–
1180 W245. https://doi.org/10.1093/nar/gky354.

1181 50. Stewart, S.A., Dykxhoorn, D.M., Palliser, D., Mizuno, H., Yu, E.Y., An, D.S., Sabatini, D.M.,
1182 Chen, I.S.Y., Hahn, W.C., Sharp, P.A., et al. (2003). Lentivirus-delivered stable gene
1183 silencing by RNAi in primary cells. RNA *9*, 493–501. https://doi.org/10.1261/rna.2192803.

1184 51. Langmead, B., Trapnell, C., Pop, M., and Salzberg, S.L. (2009). Ultrafast and memory-
1185 efficient alignment of short DNA sequences to the human genome. Genome Biol *10*, R25.
1186 https://doi.org/10.1186/gb-2009-10-3-r25.

1187 52. Li, W., Xu, H., Xiao, T., Cong, L., Love, M.I., Zhang, F., Irizarry, R.A., Liu, J.S., Brown, M.,
1188 and Liu, X.S. (2014). MAGeCK enables robust identification of essential genes from
1189 genome-scale CRISPR/Cas9 knockout screens. Genome Biol *15*, 554.
1190 https://doi.org/10.1186/s13059-014-0554-4.

1191 53. R Core Team (2022). R: A Language and Environment for Statistical Computing |
1192 BibSonomy. R Foundation for Statistical Computing.

1193 54. Wei T, S.V. (2021). R package “corrplot”: Visualization of a Correlation Matrix (Version
1194 0.92). https://github.com/taiyun/corrplot.

55. Silva, D., Santos, G., Barroca, M., and Collins, T. (2017). Inverse PCR for Point Mutation Introduction. In PCR: Methods and Protocols Methods in Molecular Biology., L. Domingues, ed. (Springer), pp. 87–100. https://doi.org/10.1007/978-1-4939-7060-5_5.

Supplement

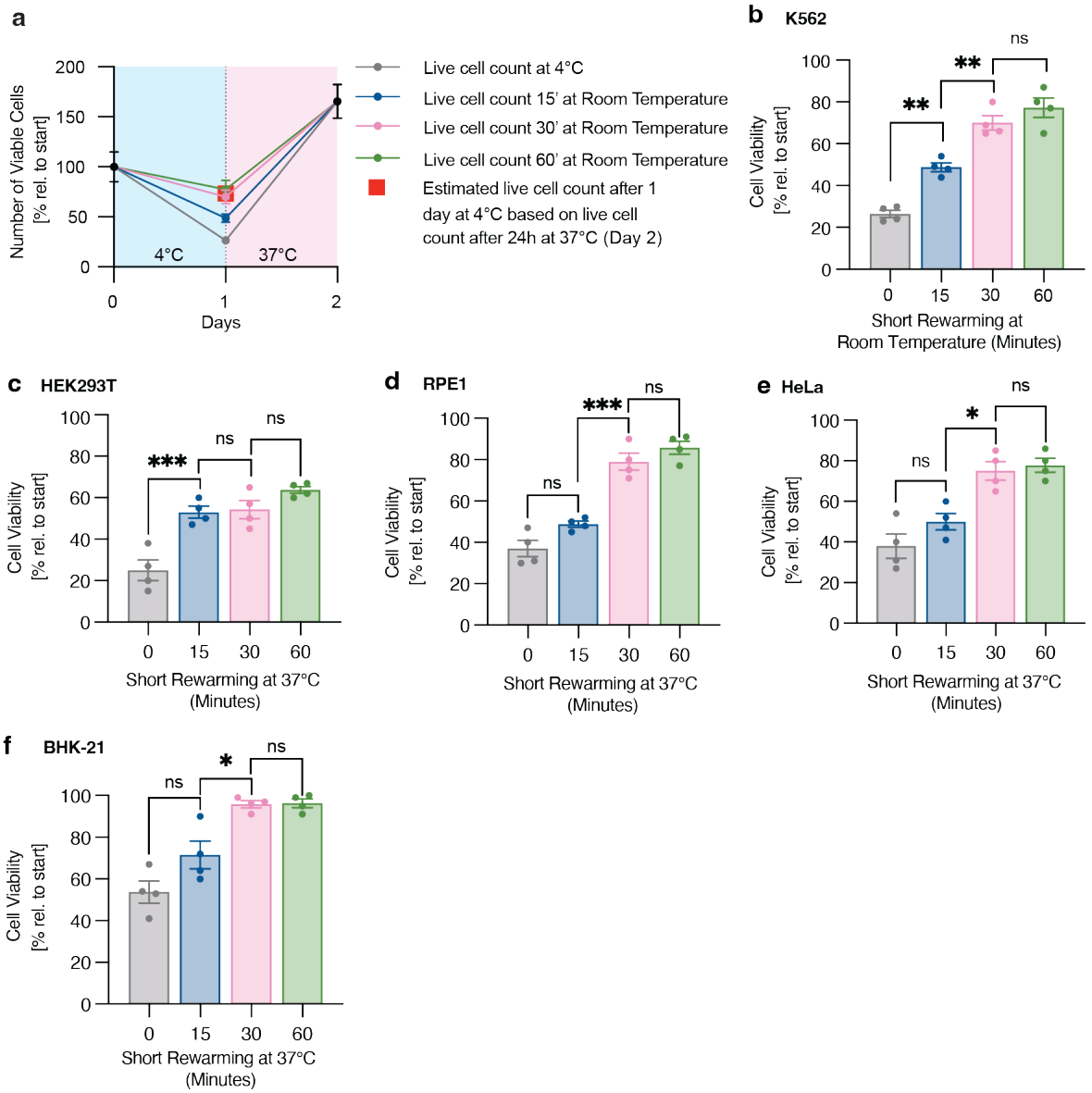

Supplement 1. Permeability to trypan blue changes rapidly upon cell rewarming

a, Number of viable K562 cells based on trypan blue staining after one day at 4°C and subsequent rewarming for 24 hours at 37°C. Numbers are normalized to initial cell counts. Dots indicate viable cell number based on trypan blue staining of cells after incubation at room temperature for 15, 30, or 60 minutes. Blue shaded regions indicate 4°C exposure and shaded

1206 pink regions indicate 37°C exposure. Red square indicates calculated cell counts after one day
1207 at 4°C based on the viable cell number measured after 24 hour rewarming. **b**, Viability of K562
1208 cells was assessed by trypan blue staining after incubation at room temperature for 0, 15, 30, or
1209 60 minutes following 24 hours at 4°C (n = 4). Cells incubated at room temperature for 15
1210 minutes show a significant increase in cell counts compared to cells counted immediately (**P =
1211 0.0016). Cells incubated at room temperature for 30 minutes show a significant increase in cell
1212 counts compared to a 15-minute incubation (**P = 0.0023), while no significant difference in
1213 viability was observed between cells incubated for 30 or 60 minutes (ns, P = 0.4059). **c-f**,
1214 Viability of cells was assessed by trypan blue staining after incubation at 37°C for 0, 15, 30, or
1215 60 minutes following 24 hours at 4°C (n = 4). **c**, HEK293T, **d**, RPE1, **e**, HeLa, **f**, BHK-21. No
1216 significant difference in cell viability was observed between cells incubated for 30 or 60 minutes
1217 for HEK293T (ns, P = 0.3122), RPE1 (ns, P = 0.5137), HeLa (ns, P = 0.9735), and BHK-21 (ns,
1218 P = 0.9998) cells. All values show mean ± SEM, with significance determined by one-way
1219 ANOVA adjusted for multiple comparisons by Tukey's HSD. *P < 0.05; **P < 0.01; ***P < 0.001;
1220 ****P < 0.0001; ns P > 0.05.
1221

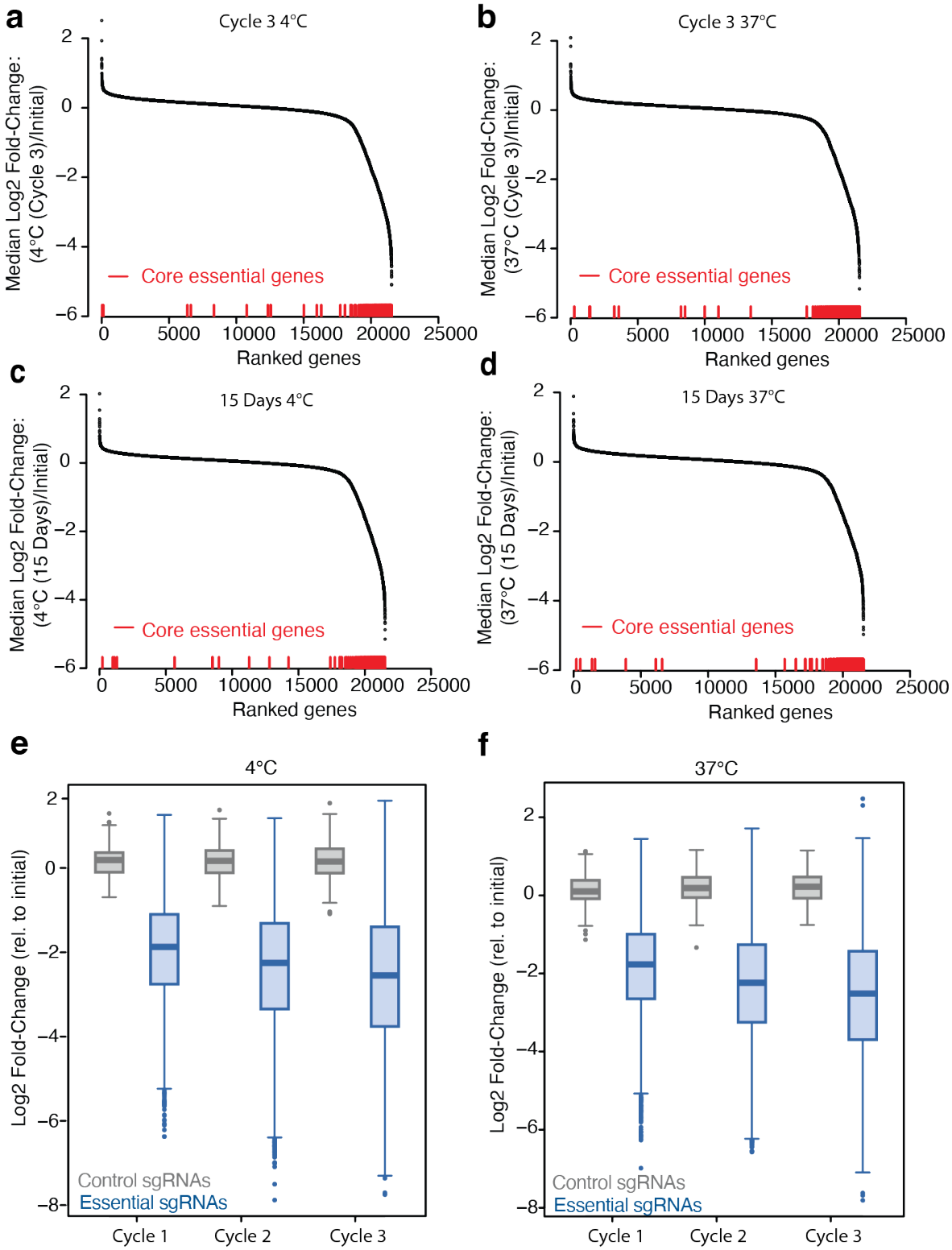

Supplement 2. Depletion of Core Essential Genes in Genome-Wide BHK-21 Screens

a-d, Genes ranked by median fold-change (log2) in genome-wide BHK-21 screens. **a**, after three cycles of cold exposure and rewarming (Cycle 3 4°C), **b**, matched constant 37°C control

1226 condition (Cycle 3 37°C), **c**, after 15 days of 4°C exposure (15 Days 4°C), **d**, matched constant
1227 37°C control condition (15 Days 37°C). Core essential genes[24] indicated in red are positioned
1228 below based on gene rank to demonstrate their depletion in each screen condition. **e-f**, Boxplots
1229 showing log2 fold change in representation for the population of control sgRNAs (gray; n = 250)
1230 or sgRNAs targeting core essential genes[24] (blue; n = 4635) over **e)** three cycles of cold
1231 exposure and rewarming (4°C) or **f)** constant 37°C control conditions. The line within each box
1232 represents the median, the bounds of each box represent the first and third quartiles, and the
1233 whiskers extend to the furthest data point within 1.5 times the interquartile range. A two-sided
1234 Kolmogorov-Smirnov test was used to test the difference between each pair of control/essential-
1235 gene-targeting sgRNA distributions (estimated p-value < 2.2e-16 for all six pairs in e and f).
1236

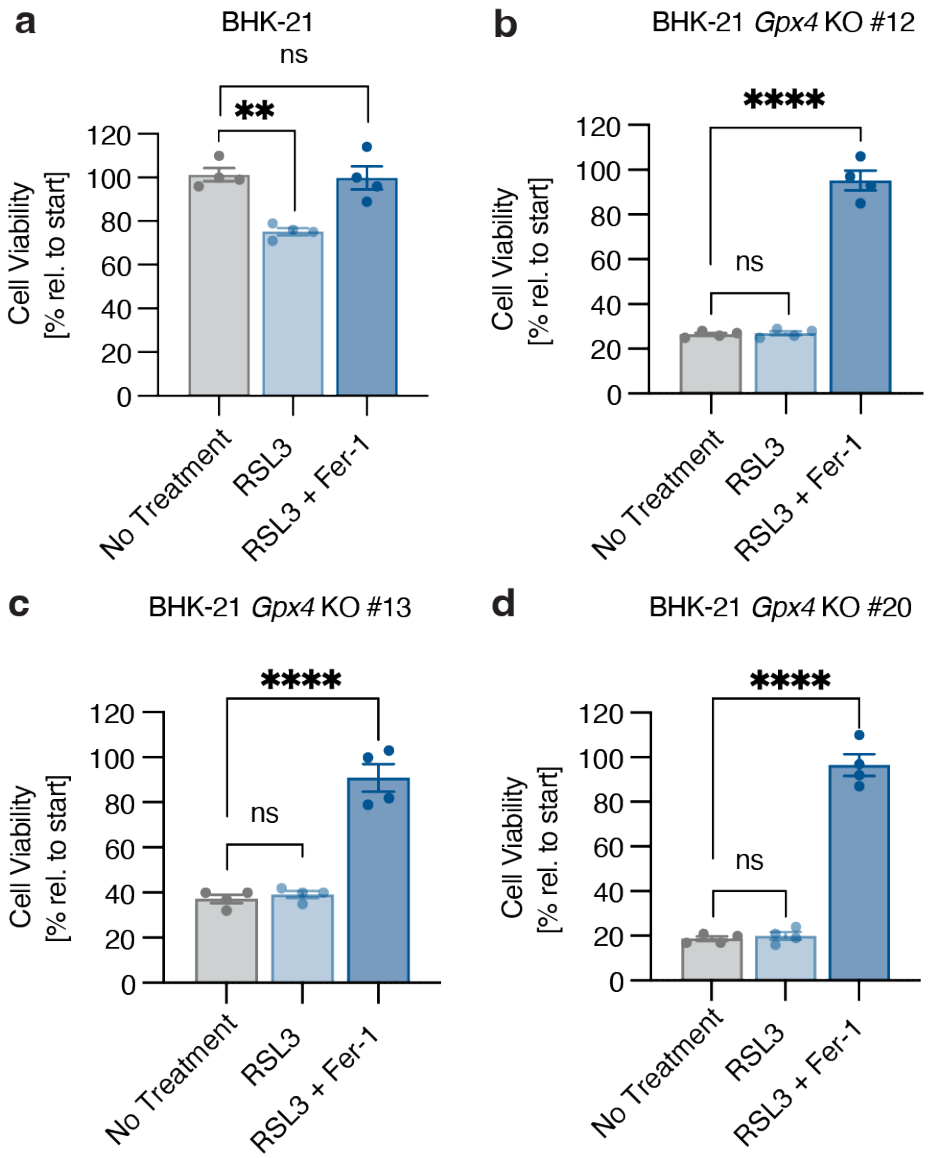

Supplement 3. RSL3 treatment has no effect on the viability of cold-exposed *Gpx4* KO BHK-21 cells.

a-d, Wild-type BHK-21 cells **(a)** and three independent *Gpx4* KO BHK-21 clonal lines **(b-d)** were treated with RSL3 (1 μM) and ferrostatin-1 (Fer-1, 1 μM) as indicated for 24 hours at 4°C (n = 4) prior to trypan blue staining. Wild-type BHK-21 cells show a significant decrease in cell viability when treated with RSL3 compared to no treatment (**P = 0.0013), whereas *Gpx4* KO lines show no significant changes in viability (ns, P > 0.05). All values show mean ± SEM, with significance measured by one-way ANOVA adjusted for multiple comparisons by Dunnett's test. *P < 0.05; **P < 0.01; ***P < 0.001; ****P < 0.0001; ns P > 0.05.

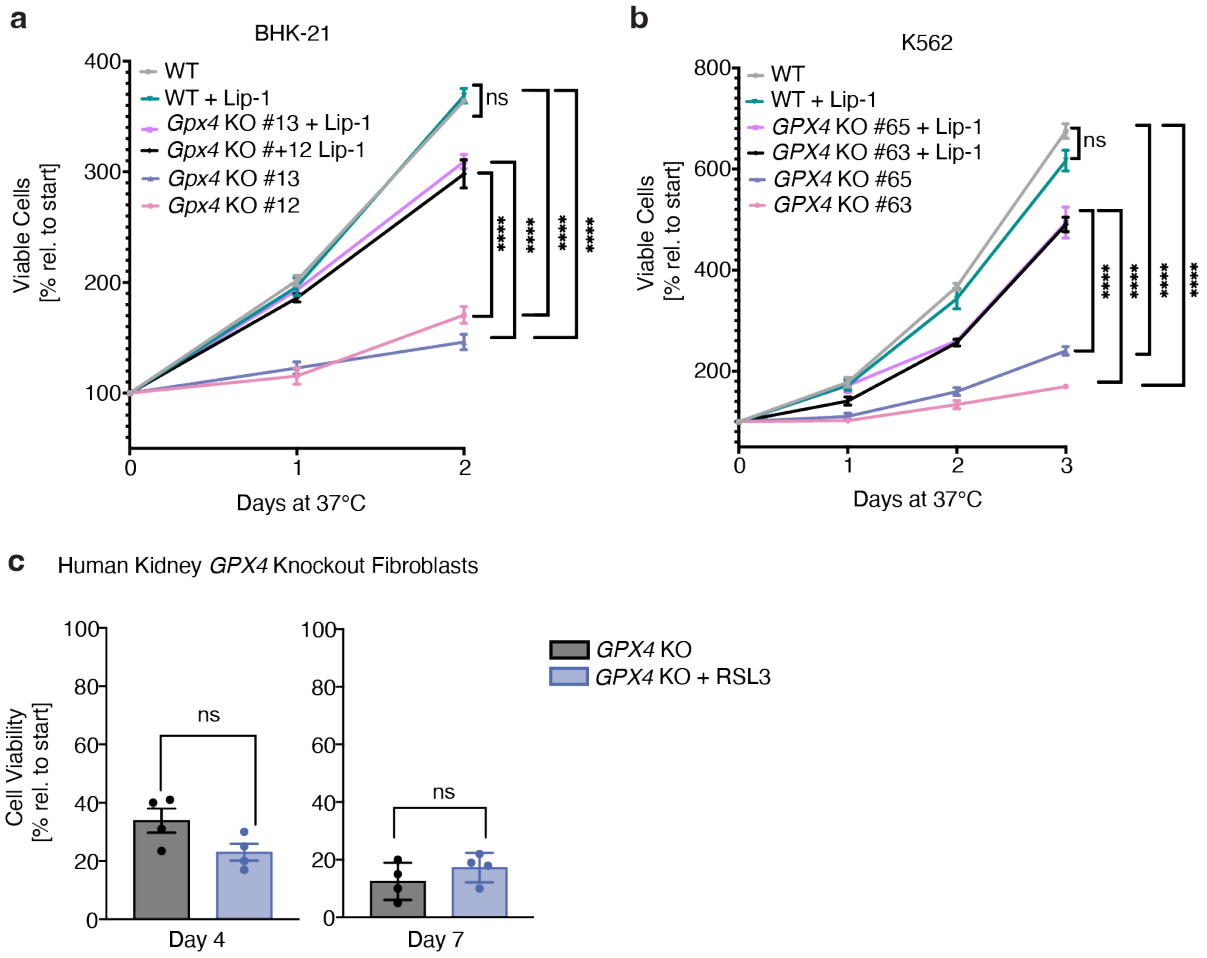

Supplement 4. Growth of BHK21 and K562 *GPX4* knockout cells and effects of RSL3 treatment on human kidney fibroblast *GPX4* knockout cells

a, Viable K562 cells recorded as percentage relative to start based on trypan blue staining over the course of 3 days at 37°C. Cell growth is significantly decreased in *GPX4* K562 KO clones compared to WT K562 cells. Supplementation of liproxstatin-1 (2.5 μM) increases cell viability in *GPX4* KO cells and not WT cells at 37°C. **b**, Viable BHK-21 cells recorded as percentage relative to start based on trypan blue staining over the course of 2 days. Cell growth is significantly decreased in *Gpx4* BHK-21 KO cells compared to WT BHK-21 cells. Supplementation of liproxstatin-1 (2.5 μM) increases cell viability in *Gpx4* KO cell and not WT cells at 37°C. **c**, Human kidney GPX4 KO cells were placed at 4°C and left untreated or treated with RSL3 (1 μM) for 4, and 7 days (n = 4). Treatment with RSL3 does not confer significant additional death (n=4 per timepoint and condition) as measure by two-tailed t-test. All values show mean ± SEM, with significance measured by one-way ANOVA adjusted for multiple

1262 comparisons with Tukey's HSD unless otherwise specified. *$P < 0.05$; **$P < 0.01$; ***$P < 0.001$;
1263 ****$P < 0.0001$; ns $P > 0.05$.
1264
1265
1266
1267
1268
1269
1270

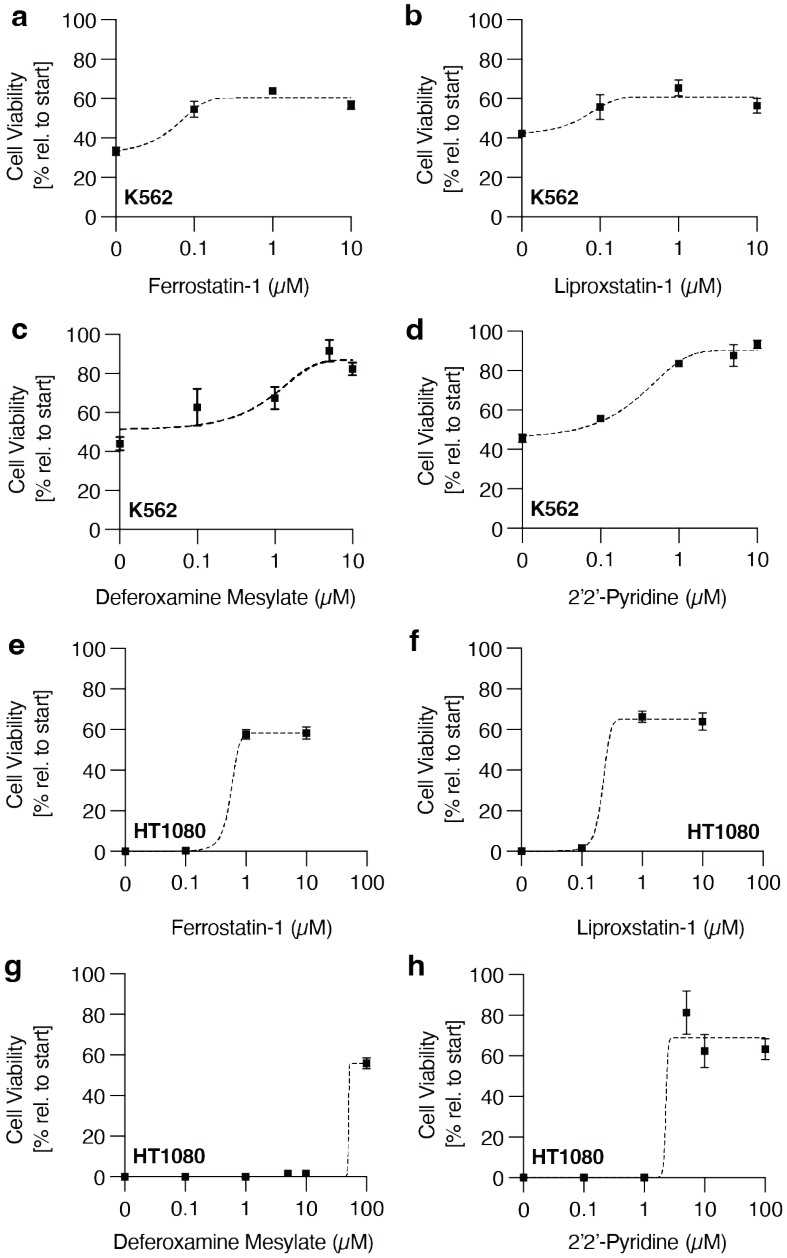

1271

1272

1273 **Supplement 5. Ferroptosis inhibitors and iron chelators increase cold cell viability in a**

1274 **dose-dependent manner**

1275 **a-h**, K562 **(a-d)** and HT1080 **(e-h)** cells were treated with varying concentrations of the

1276 ferroptosis inhibitors, ferrostatin-1 and liproxstatin-1, and iron chelators, deferoxamine and 2'2'-

1277 pyridine, for four days at 4°C prior to assaying cell viability by trypan blue staining (n = 3). All

1278 values show mean ± SEM.

1279

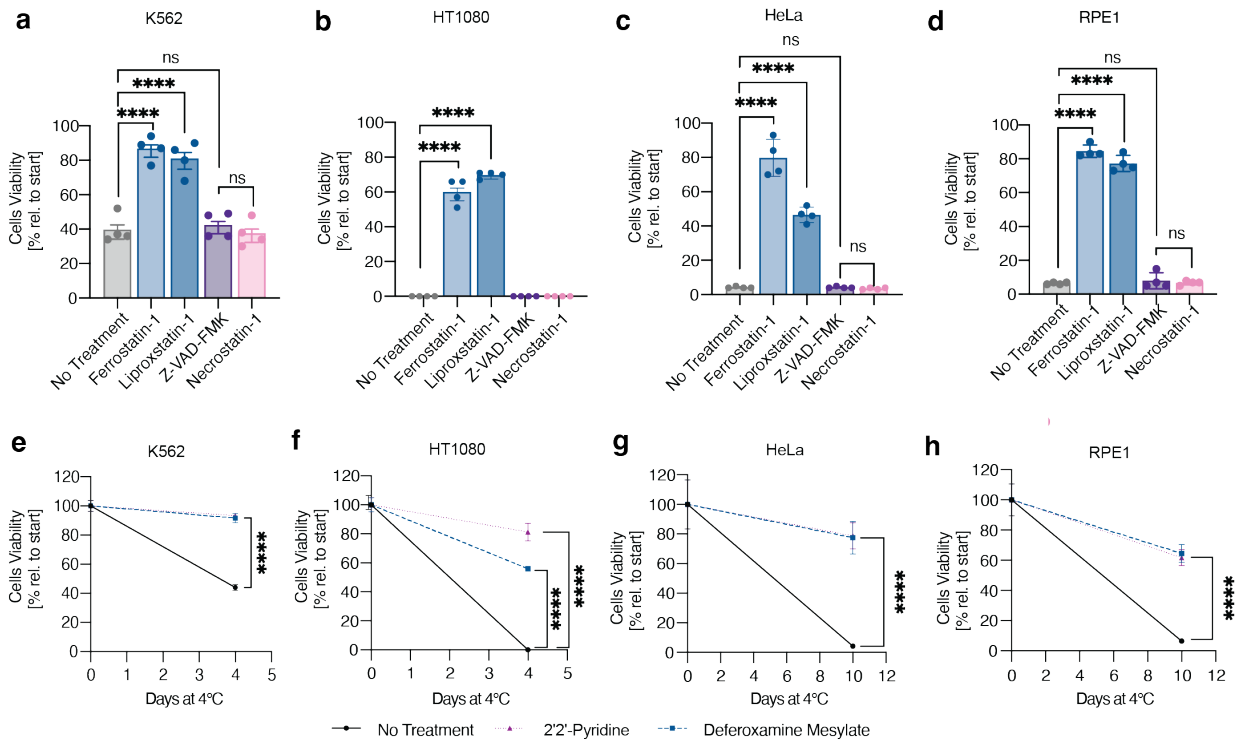

Supplement 6. Cells derived from non-hibernators undergo cold-induced ferroptotic cell death

a, K562 cells were treated with ferrostatin-1 (1 μM) (****$P < 0.0001$), liproxstatin-1 (1 μM) (****$P < 0.0001$), Z-VAD-FMK (1 μM) (ns, $P = 0.9760$), or necrostatin-1 (1 μM) (ns, $P = 0.9835$) for 4 days at 4°C prior to trypan blue staining ($n = 4$). **b**, HT1080 cells treated with ferrostatin-1 (1 μM) (****$P < 0.0001$), liproxstatin-1 (1 μM) (****$P < 0.0001$), Z-VAD-FMK (1 μM), or necrostatin-1 (1 μM) for 4 days at 4°C prior to trypan blue staining ($n = 4$). **c**, HeLa cells treated with ferrostatin-1 (1 μM) (****$P < 0.0001$), liproxstatin-1 (1 μM) (****$P < 0.0001$), Z-VAD-FMK (1 μM) (ns, $P > 0.9999$), or necrostatin-1 (1 μM) (ns, $P = 0.9987$) for 10 days at 4°C prior to trypan blue staining ($n = 4$). **d**, RPE1 cells treated with ferrostatin-1 (1 μM) (****$P < 0.0001$), liproxstatin-1 (1 μM) (****$P < 0.0001$), Z-VAD-FMK (1 μM) (ns, $P = 0.9291$), or necrostatin-1 (1 μM) (ns, $P > 0.9999$) for 10 days at 4°C prior to trypan blue staining ($n = 4$). **e**, K562 cells treated with deferoxamine mesylate (5 μM) (***$P = 0.0002$) or 2'2'-pyridine (10 μM) (****$P < 0.0001$) for 4 days at 4°C prior to trypan blue staining ($n = 3$). **f**, HT1080 cells treated with deferoxamine mesylate (100 μM) (****$P < 0.0001$) or 2'2'-pyridine (5 μM) (***$P = 0.0002$) for 4 days at 4°C prior to trypan blue staining ($n = 3$). **g**, HeLa cells treated with deferoxamine mesylate (5 μM) (****$P < 0.0001$) or 2'2'-pyridine (5 μM) (****$P < 0.0001$) for 10 days at 4°C prior to trypan blue staining ($n = 3$). **h**,

1299 RPE1 cells treated with deferoxamine mesylate (100 μM) (****$P < 0.0001$) or 2'2'-pyridine (5
1300 μM) (***$P < 0.0001$) for 10 days at 4°C prior to trypan blue staining ($n = 3$). All values show
1301 mean ± SEM, with significance measured one-way ANOVA adjusted for multiple comparisons
1302 by Dunnett's test. *$P < 0.05$; **$P < 0.01$; ***$P < 0.001$; ****$P < 0.0001$; ns $P > 0.05$.
1303

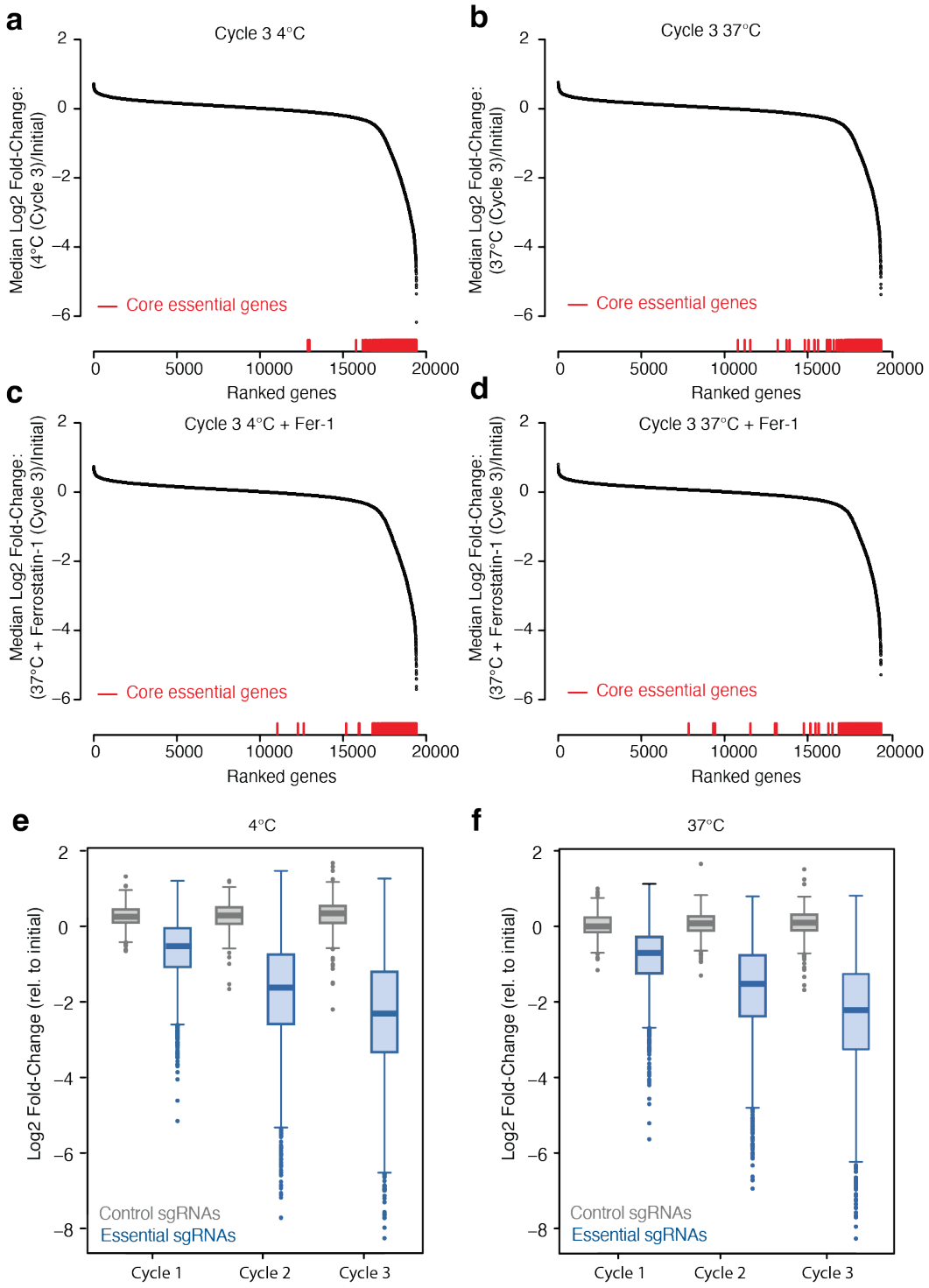

Supplement 7. Depletion of Core Essential Genes in Genome-Wide K562 Screens

a-d, Genes ranked by median fold-change (log2) in genome-wide K562 screens. **a**, after three cycles of cold exposure (Cycle 3 4°C), **b**, matched constant 37°C control condition (Cycle 3

37°C), **c**, three cycles of cold exposure with 1 μM ferrostatin-1 (Cycle 3 4°C + Fer-1), **d**, matched constant 37°C control condition with 1 μM ferrostatin-1 (Cycle 3 37°C + Fer-1). Core essential genes[24] (red bars) are positioned below based on gene rank to demonstrate their depletion in each screen condition. **e-f**, Boxplots showing the log2 fold change in representation for the population of control sgRNAs (gray; n = 500) or sgRNAs targeting core essential genes[24] (blue; n = 3219) over **e)** three cycles of cold exposure (4°C) or **f)** constant 37°C control conditions. The line within each box represents the median, the bounds of each box represent the first and third quartiles, and the whiskers extend to the furthest data point within 1.5 times the interquartile range. A two-sided Kolmogorov-Smirnov test was used to test the difference between each pair of control/essential-gene-targeting sgRNA distributions (estimated p-value < 2.2e-16 for all six pairs in e and f).

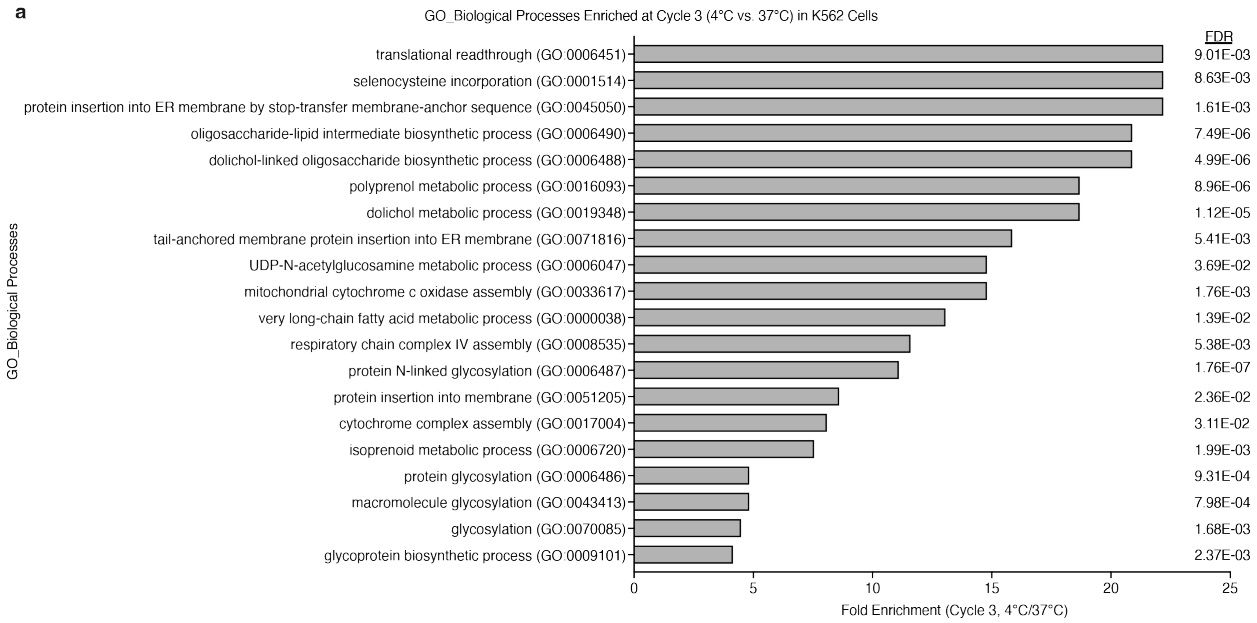

Supplement 8. Top 20 enriched pathways at Cycle 3 (4°C vs. 37°C) in K562 cells

a, Graphical representation of the top 20 enriched, differentially expressed gene sets (204 genes; FDR < 0.1) from the genome-scale CRISPR-Cas9 screen in K562 cells (Cycle 3 4°C vs. 3 passages at 37°C). GO_Biological Processes Panther overrepresentation test was used to determine enriched gene sets. Functional annotation analysis of the selectively required genes identified pathways related to translational readthrough, selenocysteine incorporation, protein insertion into the ER, glycosylation, fatty acid metabolism, and mitochondrial respiration. A full list of pathways is provided in Table S6.

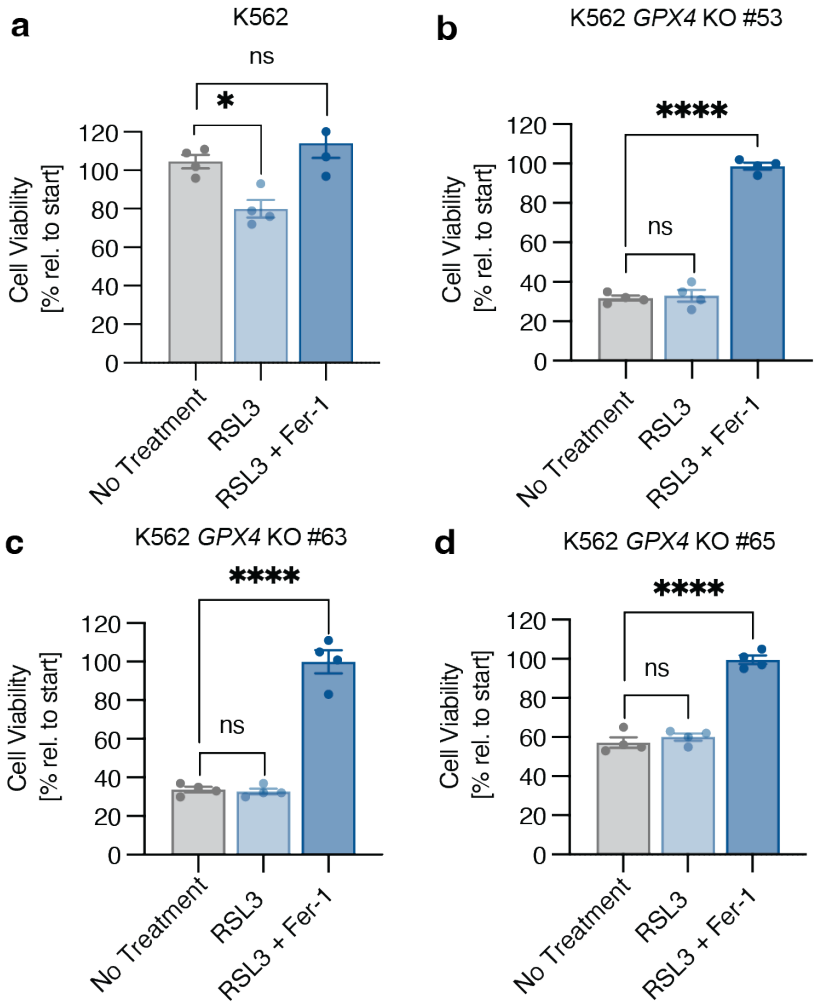

Supplement 9. RSL3 treatment has no effect on the viability of cold-exposed *GPX4* KO K562 cells.

a-d, Wild-type K562 cells **(a)** and three independent *GPX4* KO K562 clonal lines **(b-d)** were treated with RSL3 (1 μM) and ferrostatin-1 (Fer-1, 1 μM) as indicated for 8 hours at 4°C (n = 4) prior to trypan blue staining. Wild-type K562 cells show a significant decrease in cell viability when treated with RSL3 compared to no treatment (*P = 0.0213), whereas *GPX4* KO lines show no significant changes in viability (ns, P > 0.05). All values show mean ± SEM, with significance measured by one-way ANOVA adjusted for multiple comparisons by Dunnett's test. *P < 0.05; **P < 0.01; ***P < 0.001; ****P < 0.0001; ns P > 0.05.

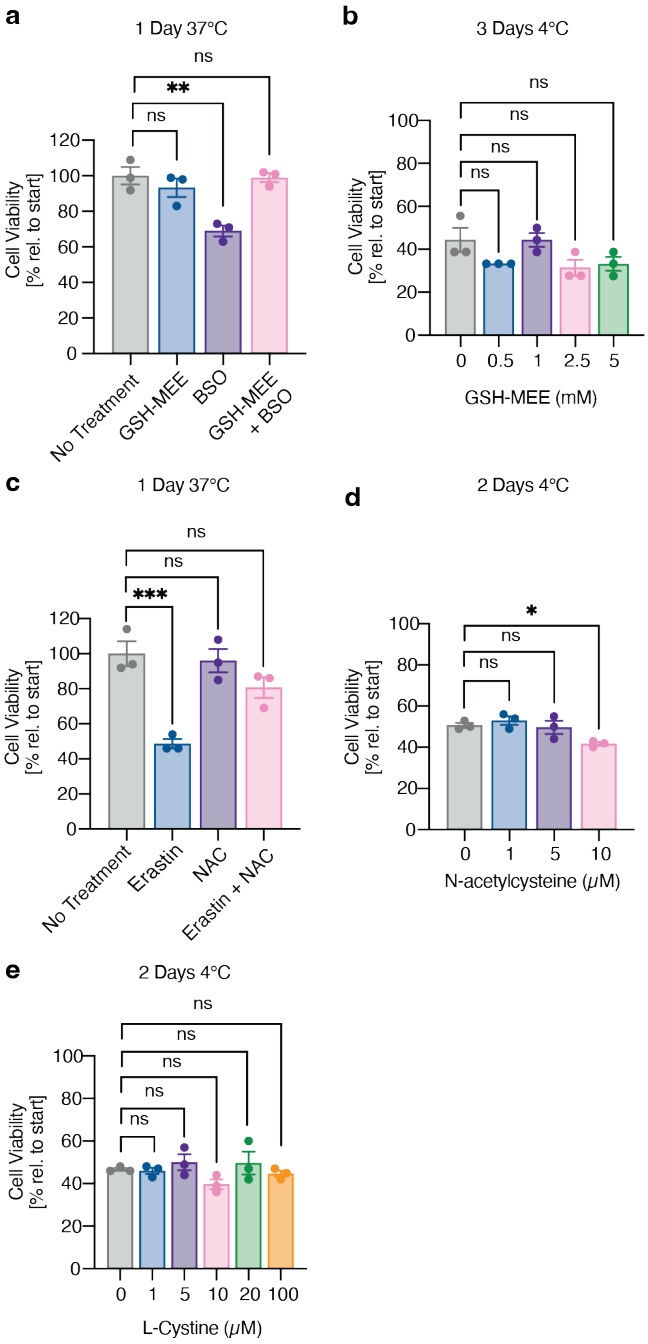

Supplement 10. Cell permeable glutathione and glutathione precursors do not increase cold cell viability

a, K562 cells were placed at 37°C and treated with cell permeable glutathione GSH-MEE (1 μM) and/or the glutathione synthesis inhibitor buthionine sulfoximine (BSO, 1 μM) for 1 day (n = 3). Treatment with BSO resulted in increased cell death (**P = 0.0018) that was rescued by GSH-MEE (ns, P = 0.9961). **b,** Treatment with GSH-MEE has no effect on K562 cold-induced death

after 3 days at 4°C as measured by trypan blue staining (n = 3, 5 μM; ns, P = 0.1558). **c,** K562 cells were placed at 37°C and treated with ferroptosis inducer Erastin (10 μM) and N-acetylcysteine (NAC, 10 μM) for 1 day (n = 3). Treatment with Erastin resulted in increased cell death (***P = 0.0006) that was rescued by NAC (ns, P = 0.1091). **d,** Treatment with N-acetylcysteine does not increase cold cell viability in K562 cells after 2 days at 4°C as measured by trypan blue staining (n = 3, 10 μM; *P = 0.0352). **e,** Treatment with L-Cystine does not increase cold cell viability in K562 cells after 2 days at 4°C as measured by trypan blue staining (n = 3, 100 μM; ns, P = 0.9843). All values show mean ± SEM, with significance measured by one-way ANOVA adjusted for multiple comparisons by Dunnett's test. *P < 0.05; **P < 0.01; ***P < 0.001; ****P < 0.0001; ns P > 0.05.

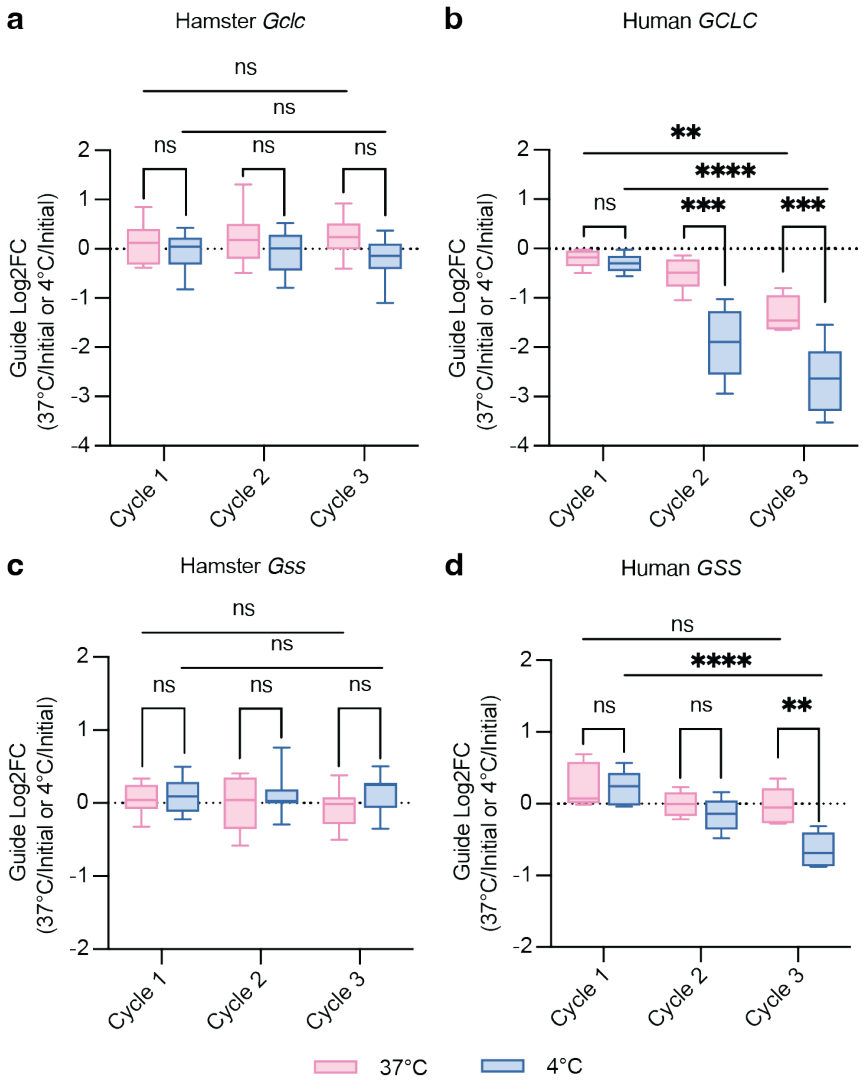

Supplement 11. Glutathione biosynthesis genes show increased depletion in cold-exposed K562 cells

a,c, Log2 fold-change (log2FC) of 10 guides per targeted gene in BHK-21 genome-wide screen, showing guide depletion over three cycles of cold exposure and rewarming. **a**, *Gclc*, **c**, *Gss*. **b**, **d**, Log2 fold-change (log2FC) of 5 guides per targeted gene in K562 genome-wide screen, showing significant guide depletion over three cycles of cold exposure. **b**, *GCLC*, **d**, *GSS*. Significance between Cycle 1 versus Cycle 3 is measured by two-way ANOVA adjusted for multiple comparisons by Dunnett's test. Significance between 37°C and 4°C for each cycle is measured by two-way ANOVA adjusted for multiple comparisons by Bonferroni's test. *$P < 0.05$; **$P < 0.01$; ***$P < 0.001$; ****$P < 0.0001$; ns $P > 0.05$.